

MTRB LIBRARY

SECOND

Progress Report  
(PROJECT SR-119)

on

**WELDED REINFORCEMENT OF OPENINGS  
IN STRUCTURAL STEEL MEMBERS:**

A Determination of Strain Energy Distribution  
And True Stresses In The Plastic Range  
In Plates With Openings

by

D. VASARHELYI AND R. A. HECHTMAN  
University of Washington  
Under Bureau of Ships Contract NObs-50238  
(Index No. NS-731-034)

for

**SHIP STRUCTURE COMMITTEE**

Convened by  
The Secretary of the Treasury

*Member Agencies—Ship Structure Committee*

Bureau of Ships, Dept. of Navy  
Military Sea Transportation Service, Dept. of Navy  
United States Coast Guard, Treasury Dept.  
Maritime Administration, Dept. of Commerce  
American Bureau of Shipping

*Address Correspondence To:*

Secretary  
Ship Structure Committee  
U. S. Coast Guard Headquarters  
Washington 25, D. C.

SERIAL NO. SSC-50

MARCH 10, 1952

# SHIP STRUCTURE COMMITTEE

March 10, 1952

**MEMBER AGENCIES:**

BUREAU OF SHIPS, DEPT. OF NAVY  
MILITARY SEA TRANSPORTATION SERVICE, DEPT. OF NAVY  
UNITED STATES COAST GUARD, TREASURY DEPT.  
MARITIME ADMINISTRATION, DEPT. OF COMMERCE  
AMERICAN BUREAU OF SHIPPING

**ADDRESS CORRESPONDENCE TO:**

SECRETARY  
SHIP STRUCTURE COMMITTEE  
U. S. COAST GUARD HEADQUARTERS  
WASHINGTON 25, D. C.


Dear Sir:

Herewith is a copy of the second Progress Report entitled, "Welded Reinforcement of Openings in Structural Steel Members: A Determination of Strain Energy Distribution and True Stresses in the Plastic Range in Plates with Openings" by D. Vasarhelyi and R. A. Hechtman. This investigation is being conducted at the University of Washington for the Ship Structure Committee and covers work completed between August 1950 and August 1951.

Any questions, comments, criticism or other matters pertaining to the Report should be addressed to the Secretary, Ship Structure Committee.

This Report is being distributed to those individuals and agencies associated with and interested in the work of the Ship Structure Committee.

Yours sincerely,

  
K. K. COWART  
Rear Admiral, U. S. Coast Guard  
Chairman, Ship Structure  
Committee

PROGRESS REPORT

(SECOND)

WELDED REINFORCEMENT OF OPENINGS  
IN STRUCTURAL STEEL MEMBERS

by

D. Vasarhelyi and R. A. Hechtman  
University of Washington

for

SHIP STRUCTURE COMMITTEE

Under Navy Contract NObs-50238

Index No. NS731-034

## TABLE OF CONTENTS

| <u>Contents</u>   | <u>Page</u> |
|---|-------------|
| I. ABSTRACT   | 1           |
| II. OBJECT AND SCOPE OF INVESTIGATION   | 2           |
| III. UNIT STRAIN ENERGY DISTRIBUTION IN THE PLASTIC RANGE OF THE MATERIAL DETERMINED BY THE OCTAHEDRAL THEORY | 2           |
| IV. EXPERIMENTAL DETERMINATION OF TRUE STRESSES BY USE OF TENSILE TEST DATA                                   | 6           |
| V. TEST SPECIMENS AND TEST METHODS  | 8           |
| 1. Chemical Analysis and Mechanical Properties  | 8           |
| 2. Calibration Tensile Specimens  | 9           |
| 3. Plates with square opening with Rounded Corners  | 9           |
| VI. CALIBRATION TENSILE TESTS   | 11          |
| 1. Procedure for Computing the Unit Energy Absorption   | 11          |
| 2. Determination of Poisson's Ratio and the Tangent Modulus   | 12          |
| VII. PILOT TEST AT LOW TEMPERATURE OF PLATE WITH SQUARE OPENING WITH ROUNDED CORNERS                          | 13          |
| VIII. TEST OF TWO LARGE PLATES WITH SQUARE OPENING WITH ROUNDED CORNERS                                       | 13          |
| 1. Tests and Type of Fracture   | 13          |
| 2. Computation of the Unit Strain Energy Distribution by the Octahedral Theory                                | 14          |
| 3. Rate of Increase of Unit Energy Absorption   | 17          |
| 4. Computation of the True Stress Distribution on Transverse Cross-Sections at the Ultimate Load              | 20          |
| IX. SUMMARY AND CONCLUSIONS   | 23          |
| X. SYMBOLS  | 25          |
| XI. ACKNOWLEDGMENTS   | 26          |

## LIST OF FIGURES

| <u>FIG. NO.</u> | <u>TITLE</u>  |
|-----------------|---|
| 1               | Graphical Definition of $E_T$ and $\beta$ .   |
| 2               | Sketch of Tensile Calibration Test Specimen.  |
| 3               | Plate with Square Opening with Rounded Corners.   |
| 4               | Cooling Chamber Enclosing the Plate Specimen.   |
| 5               | Location of Grid and Slide-Wire Gages.  |
| 6               | Calibration Test True Stress-Strain Curves.   |
| 7               | Relation of Unit Strain Energy Absorption and Octahedral Shear Strain for Calibration Test Specimens.   |
| 8               | Plot of Poisson's Ratio as a Function of True Stress in Plastic Range of Calibration Test Specimen, 76 Deg. F.  |
| 9               | Plot of Poisson's Ratio as a Function of True Stress in Plastic Range of Calibration Test Specimen, -20 Deg. F.   |
| 10              | Plot of $E_T$ as a Function of Natural Strain.  |
| 11              | Load-Average Elongation Curves for Plates with Square Opening with Rounded Corners.   |
| 12              | Photographs of Plates after Failure.  |
| 13              | Unit Strain Energy Contours for Plate with Square Opening with Rounded Corners for Load of 500 kips, 63 Per Cent of Maximum Load. Spec. No. 37. Temperature 76 Deg. F.  |
| 14              | Unit Strain Energy Contours for Plate with Square Opening with Rounded Corners for Load of 650 kips, 81 Per Cent of Maximum Load. Spec. No. 37. Temperature 76 Deg. F.  |
| 15              | Unit Strain Energy Contours for Plate with Square Opening with Rounded Corners for Load of 720 kips, 90 per cent of Maximum Load. Spec. No. 37. Temperature 76 Deg. F.  |
| 16              | Unit Strain Energy Contours for Plate with Square Opening with Rounded Corners for Load of 800 kips, 100 Per Cent of Maximum Load. Spec. No. 37. Temperature 76 Deg. F. |

LIST OF FIGURES (Cont.)

| <u>Fig. No.</u> | <u>Title</u>   |
|-----------------|--|
| 17              | Unit Strain Energy Contours for Plate with Square Opening with Rounded Corners for Load of 500 kips, 55 Per Cent of Maximum Load. Spec. No. 38. Temperature -20 Deg. F.  |
| 18              | Unit Strain Energy Contours for Plate with Square Opening with Rounded Corners for Load of 650 kips, 71 Per Cent of Maximum Load. Spec. No. 38. Temperature -20 Deg. F.  |
| 19              | Unit Strain Energy Contours for Plate with Square Opening with Rounded Corners for Load of 720 kips, 79 Per Cent of Maximum Load. Spec. No. 38. Temperature -20 Deg. F.  |
| 20              | Unit Strain Energy Contours for Plate with Square Opening with Rounded Corners for Load of 800 kips, 87 Per Cent of Maximum Load. Spec. No. 38. Temperature -20 Deg. F.  |
| 21              | Unit Strain Energy Contours for Plate With Square Opening with Rounded Corners for Load of 870 kips, 95 Per Cent of Maximum Load. Spec. No. 38. Temperature -20 Deg. F.  |
| 22              | Unit Strain Energy Contours for Plate With Square Opening with Rounded Corners for Load of 915 kips, 100 Per Cent of Maximum Load. Spec. No. 38. Temperature -20 Deg. F. |
| 23              | Comparison of Total Strain Energy and Applied Load for Plates with Square Openings with Rounded Corners.   |
| 24              | Growth of Unit Strain Energy at Typical Points on Specimens Under Applied Load. Spec. Nos. 37 and 38.  |
| 25              | Contours of the Equal Rates of Energy Absorption. Spec. No. 37.  |
| 26              | Contours of the Equal Rates of Energy Absorption. Spec. No. 38.  |
| 27              | Distribution of True Thickness, Axial True Stress and Force Per Inch for Transverse Section a-a at Maximum Load of 800 kips. Spec. No. 37.                               |

LIST OF FIGURES (Cont.)

| <u>Fig. No.</u> | <u>Title</u>   |
|-----------------|--|
| 28              | Distribution of True Thickness, Axial True Stress and Force Per Inch for Transverse Section b-b at Maximum Load of 800 kips. Spec. No. 37. |
| 29              | Distribution of True Thickness, Axial True Stress and Force Per Inch for Transverse Section c-c at Maximum Load of 800 kips. Spec. No. 37. |
| 30              | Distribution of True Thickness, Axial True Stress and Force Per Inch for Transverse Section d-d at Maximum Load of 800 kips. Spec. No. 37. |
| 31              | Distribution of True Thickness, Axial True Stress and Force Per Inch for Transverse Section a-a at Maximum Load of 915 kips. Spec. No. 38. |
| 32              | Distribution of True Thickness, Axial True Stress and Force per Inch for Transverse Section b-b at Maximum Load of 915 kips. Spec. No. 38. |
| 33              | Distribution of True Thickness, Axial True Stress and Force Per Inch for Transverse Section c-c at Maximum Load of 915 kips. Spec. No. 38. |
| 34              | Distribution of True Thickness, Axial True Stress and Force Per Inch for Transverse Section d-d at Maximum Load of 915 kips. Spec. No. 38. |

pg 1+2

A DETERMINATION OF STRAIN ENERGY DISTRIBUTION  
AND TRUE STRESSES IN THE PLASTIC RANGE  
IN PLATES WITH OPENINGS

I. ABSTRACT

The research reported herein is a part of the investigation of welded reinforcement of openings in structural steel members. A previous report<sup>1</sup> described the tests of 1/4-in. plates with and without welded reinforcement. The purpose of the tests covered by this report was to determine the unit strain energy and the true stress distribution in the plastic range of the material in a flat plate with a centrally located opening, which was square with rounded corners. Two such plates made from plain-carbon semi-killed structural steel were tested in tension, one at room temperature and the other at a temperature of -20 Deg. F.

The octahedral theory<sup>2</sup> was used to determine the unit strain energy distribution, while the true stresses were computed by a method developed in the course of the investigation. Both types of analyses utilized the experimental data of the tests as the basis of the computations. It was impossible to check the unit

---

<sup>1</sup>D. Vasarhelyi and R. A. Hechtman, First Progress Report, Welded Reinforcement of Openings in Structural Steel Members, Ship Structure Committee, Report SSC-39, Dec. 15, 1951

<sup>2</sup>A. Nadai, Energy of Distortion Absorbed by Plastic Deformation of Thin Steel Plates, Research Report SR-182, Westinghouse Research Laboratories, April, 1943.

A. Nadai, Theory of Flow and Fracture of Solids, McGraw-Hill, 1950



strain energy and true stress distributions directly, but when these were integrated in a specified manner, the total energy absorption and the load on cross-sections of the plate were obtained. These, when compared with the experimentally determined values of total energy absorption at different loads and with the testing machine load at the ultimate load gave reasonably good checks.

## II. OBJECT AND SCOPE OF INVESTIGATION

The object of the investigation was to determine the applicability of the octahedral theory<sup>2</sup> and a new method for obtaining true stresses in a notched plate which sustained large plastic strains over the entire area of the test section. These two methods were applied to two identical plate specimens, one of which failed with a completely shear fracture and the other with a fracture almost entirely cleavage.

## III. UNIT STRAIN ENERGY DISTRIBUTION IN THE PLASTIC RANGE OF THE MATERIAL DETERMINED BY THE OCTAHEDRAL THEORY

The octahedral theory, whose application to the problem of plastic distortion was suggested by A. Nadai,<sup>2</sup> utilizes the convenient relations between the octahedral shear stress and the octahedral shear strain in expressing the stress-strain condition at a point in a multi-axial stress field and from these quantities develops the unit energy absorption at the point. A previous

---

<sup>2</sup>Ibid, page 1.

application<sup>3</sup> of this method to the plastic distortion of two structural steel plates with a severe stress-raiser yielded results which checked well with measured values.

Only a brief discussion of the method will be presented here. By the equilibrium of forces and the geometry of the strains, the equations for the octahedral shear stress, the octahedral shear strain, and the unit strain energy at a point in the stressed body become as follows:

$$U = \frac{3}{2} \int \tau \, d\epsilon \quad (1)$$

For the condition of uniaxial stress,

$$\tau = \frac{\sqrt{2}}{3} \sigma_x \quad (2)$$

$$Y = \sqrt{2} E_x \quad (3)$$

For the condition of triaxial stress,

$$\tau = \frac{1}{3} \sqrt{(\sigma_x - \sigma_y)^2 + (\sigma_y - \sigma_z)^2 + (\sigma_z - \sigma_x)^2} \quad (4)$$

$$Y = \sqrt{\frac{8}{3}} \sqrt{E_x^2 + E_y^2 + E_z^2} \quad (5)$$

The symbols in these equations are defined in Sec. X of this report.

Because of the large deformations occurring in the plastic range, it is necessary to use true stresses and natural strains at all times in the application of these equations.

---

<sup>3</sup>S. I. Liu and S. T. Carpenter, A Study of Plastic Deformation and Fracturing by Strain Energy Distribution, Serial No. SSC-38, Ship Structure Committee, 12-20-50.

These equations are based on the following necessary assumptions:

1. Isotropic behavior of the material occurs throughout the plastic range.
2. The directions of the principal stresses and of the principal strains coincide at all times.
3. The entire strain energy is distortional energy, that is, the volume of the deformed body remains constant.

The second assumption is difficult to verify experimentally, but the validity of the remaining two assumptions may be found from the experimental data of the test. The third assumption neglects the elastic portion of the distortion which is almost always insignificant in problems of plasticity. The third assumption provides a simplification of the experimental procedure and makes easier the application of these equations to experimental problems in plasticity.

A given quantity of distortional energy in a biaxial or triaxial stress field may be produced by an infinite number of combinations of stress and strain. In a uniaxial stress field only one value of the stress and one value of the strain is present for a given value of the energy. Therefore, the unit energy absorption corresponding to measurable values of both the principal stresses and the principal strains under uniaxial stress may be applied to the multi-axial stress field, where only the principal strains may be measured. Experimentally, the procedure consists of two steps; first, the determination of the energy absorption per unit volume in a uniaxially stressed specimen such as a tensile or compression specimen for various values of the

octahedral shear strain; and, second, the determination of the values of the octahedral shear strain at different points in the specimen with the complex stress field and the assignment at each of these points of a value of energy absorption found in the uniaxially stressed specimen for an equal value of the octahedral shear strain. The two specimens must be made from the same piece of material. A more detailed description of this procedure will be given in a subsequent section of this report.

In the application of the octahedral theory to the present problem, two simplifying assumptions were made which brought a small degree of approximation into the test results:

1. The plate with an opening was considered as a plane stress problem, in that the stress in the direction of the thickness of the plate was neglected. This assumption involved an approximation only in a small region adjacent to the notch.
2. The principal stresses always lay in the x- and y-directions of the coordinate system. This assumption is believed to result in very small errors in the computed values of the energy absorption in all regions of the specimen except those close to the notch, where the errors in the energy values were larger but not excessively so.

#### IV. EXPERIMENTAL DETERMINATION OF TRUE STRESSES BY USE OF TENSILE TEST DATA

An experimental procedure has been devised for applying the true stress-strain relation in the simple tension or compression test to plane stress problems in plasticity. A typical true stress-strain curve for a simple tension test of a structural steel is shown in Fig. 1. The tangent to the curve at a point having the ordinates  $\bar{\sigma}$  and  $\bar{\epsilon}$  is denoted the tangent modulus of  $E_T$ , and the intercept of this tangent on the natural strain axis is called  $\beta$ .

The following two equations may be written to express the strains at a point in a plane stress problem:

$$\epsilon_x + \beta_x = \frac{\sigma_x}{E_{Tx}} - \frac{\mu_{yx}\sigma_y}{E_{Ty}} \quad (6)$$

$$\epsilon_y + \beta_y = \frac{\sigma_y}{E_{Ty}} - \frac{\mu_{xy}\sigma_x}{E_{Tx}} \quad (7)$$

Definitions of the symbols used in these equations may be found in Sec. X. These equations assume that the tangent modulus  $E_T$  remains constant in the region of the stress-strain curve in which the computation is being made - an assumption that does not introduce much approximation in this particular problem, since the true stress-strain curve for structural steel approaches linearity in the region between the end of the lower yield point range and the point where necking begins.

The simultaneous solution of Eqs. 6 and 7 gives these expressions for  $\sigma_x$  and  $\sigma_y$  :

$$\sigma_x = \frac{E_{Tx}}{1 - \mu_{xy}\mu_{yx}} \left[ (\epsilon_x + \beta_x) + \mu_{yx}(\epsilon_y + \beta_y) \right] \quad (8)$$

$$\sigma_y = \frac{E_{Ty}}{1 - \mu_{xy}\mu_{yx}} \left[ (\epsilon_y + \beta_y) + \mu_{xy}(\epsilon_x + \beta_x) \right] \quad (9)$$

Equations 8 and 9 may be rearranged as follows:

$$\sigma_x = \frac{1}{1 - \mu_{xy}\mu_{yx}} \left( \left[ E_{Tx}(\epsilon_x + \beta_x) \right] + \mu_{yx} \frac{E_{Tx}}{E_{Ty}} \left[ E_{Ty}(\epsilon_y + \beta_y) \right] \right) \quad (10)$$

$$\sigma_y = \frac{1}{1 - \mu_{xy}\mu_{yx}} \left( \left[ E_{Ty}(\epsilon_y + \beta_y) \right] + \mu_{xy} \frac{E_{Ty}}{E_{Tx}} \left[ E_{Tx}(\epsilon_x + \beta_x) \right] \right) \quad (11)$$

The quantities in the two brackets in each equation are simply the true stresses in the uniaxial true stress-strain curve,  $\overline{\sigma}_x$  and  $\overline{\sigma}_y$ , which correspond to the apparent natural strain values,  $\epsilon_x$  and

$\epsilon_y$ , measured on the specimen. Equations 10 and 11 may then be rewritten as,

$$\sigma_x = \frac{1}{1 - \mu_{xy}\mu_{yx}} \left( \overline{\sigma}_x + \mu_{yx} \frac{E_{Tx}}{E_{Ty}} \overline{\sigma}_y \right) \quad (12)$$

$$\sigma_y = \frac{1}{1 - \mu_{xy}\mu_{yx}} \left( \overline{\sigma}_y + \mu_{xy} \frac{E_{Ty}}{E_{Tx}} \overline{\sigma}_x \right) \quad (13)$$

These last two equations may be applied directly to the computation of true stresses in a plane stress problem in plasticity. The apparent natural strains,  $\epsilon_x$ , and  $\epsilon_y$ , are measured on the specimen. From the true stress-strain curves for the material tested in the x- and y-directions, the values of the true stress,  $\bar{\sigma}_x$  and  $\bar{\sigma}_y$ , corresponding to these apparent natural strains are found. When these true stress values are substituted in Eqs. 12 and 13, the true stresses,  $\sigma_x$  and  $\sigma_y$ , in the specimen are determined.

While the derivation presented here is not rigorously exact in a theoretical sense, it involves little approximation when applied to common structural metals.

#### V. TEST SPECIMENS AND TEST METHODS

##### 1. Chemical Analysis and Mechanical Properties of Steel.

All the specimens described in this report were made from the same heat of plain-carbon semi-killed steel which met ASTM Designation A-7-49T and was used in the as-rolled condition. The chemical analysis of this steel, which was called Steel U, was as follows:

| <u>C</u> | <u>Mn</u> | <u>P</u> | <u>S</u> | <u>Si</u> |
|----------|-----------|----------|----------|-----------|
| 0.23     | 0.50      | 0.053    | 0.051    | 0.07      |

The tensile properties in the direction of rolling as found from the average results of two tests of ASTM standard flat tensile specimens from each plate were as follows:

| <u>Plate No.</u> | <u>Upper Yield Point-psi</u> | <u>Ultimate Strength-psi</u> | <u>Elongation in 8 In.-per cent</u> | <u>Reduction of Area-per cent</u> |
|------------------|------------------------------|------------------------------|-------------------------------------|-----------------------------------|
| 26               | 36,900                       | 61,800                       | 34.9                                | 61.6                              |
| 4                | 34,900                       | 60,200                       | 32.2                                | 60.7                              |

The transition temperature was determined by the Navy tear test for Plate No. 4 and found to be 40 Deg. F. The plate specimens, Nos. 38 and 38A, which were tested at the lower temperatures were cut from this plate, while Spec. No. 37 came from Plate No. 26.

## 2. Calibration Tensile Specimens.

A sketch of the tensile specimen used to obtain the relation between the unit energy absorption under uniaxial stress and the octahedral shear strain is shown in Fig. 2. The blanks for these specimens were sawed from the parent plate and machined to width. Specimens cut in directions both parallel and transverse to the rolling direction were tested.

While a 12-in. gage length was used for the calibration tests, a shorter 8-in. gage length was also provided. An extensometer sensitive to a movement as small as 0.0002 in. was used to measure the elongation in 12 in. The lateral contraction of the specimen was measured with a micro-meter caliper.

For these tests at a temperature of -20 Deg. F., thermocouples were located on the specimen as shown in Fig. 2, and the specimen was jacketed with cooling tanks well beyond the gage length to insure an almost uniform temperature over the test section.

## 3. Plates with Square Opening with Rounded Corners.

Three identical specimens of the type shown in Fig. 3 were tested: the first, Spec. No. 37, at room temperature; the second, Spec. No. 38A, at a temperature of zero Deg. F. to determine the load-average elongation curve and the kind of fracture to be expected



at this temperature; and the third, Spec. No. 38, at a temperature of -20 Deg. F. The unit energy distribution over the surface of the plate and the true stresses on cross-sections of the plate were investigated in the first and third tests.

These large plates were fabricated and tested with pinned end connections in tension in a 2,400,000-lb. testing machine in the manner described in the First Progress Report.<sup>1</sup> For the low-temperature tests, the specimen and the pulling heads were enclosed in a well-insulated chamber as shown in Fig. 4, through which cold air was circulated. A mechanical refrigerator chilled the air and could be controlled within  $\pm 2$  Deg. F. The greatest difference in temperature between the center of the specimen and the end of the 36-in. long gaged section was about 15 Deg.

Spec. No. 38A was gaged with slide-wire resistance gages on 18-in. and 36-in. gage lengths and SR-4 gages.

A rectangular grid system of horizontal and vertical slide-wire resistance gages sensitive to a movement of about 0.002 in. was mounted on both faces of Specs. No. 37 and 38. These gages consisted of high-resistance wire strung through contact points mounted on the surface of the specimen. The movement of the contact points resulted in a change in the gage length, and, therefore, a change in resistance of the gage. By the measurement of this change in these calibrated gages, the elongation was determined over the surface of the plate. This grid system covered one side of the Specimen as shown in Fig. 5. In the area

---

<sup>1</sup> Ibid., page 1.

immediately above the opening where buckling of the plates occurred during testing, a similar grid was used on the other face of the plate. However, on the remainder of this latter face, a sagitta gage was employed to measure the very small amounts of curvature in these regions of the plate. This procedure reduced the number of gage lengths to be read to 214, and the readings for one load could be taken in about forty minutes. Post-yield SR-4 gages were located on the circumference of the opening on Spec. No. 37. The test was run continuously and, because of the many readings required, extended over about fifteen hours.

Since the sagitta readings on Spec. No. 37, which was tested first, indicated that bending of the plate because of initial curvature ceased by the time the specimen reached the very early stages of plastic flow, these readings were not taken on Spec. No. 38. Neither was any adjustment made in the elongation readings taken on Spec. No. 37.

A more complete description of the slide-wire resistance gages and their application will be given in a subsequent progress report.

## VI. CALIBRATION TENSILE TESTS

### 1. Procedure for Computing the Unit Energy Absorption.

The following procedure was used in obtaining the relation between the unit energy absorption in the calibration tensile specimen of the type shown in Fig. 2 and the octahedral shear strain.

- a. During the course of the test, readings of the elongation in 12 in. and the instantaneous width and thickness were taken up to the maximum load on the specimen.

- b. These data were reduced to the form of true stress-strain curves for the plates in the direction of rolling as shown in Fig. 6.
- c. From the data in Step b, the octahedral shear-stress-octahedral shear strain curve was derived by the application of Eqs. 2 and 3.
- d. The relation in Fig. 7 between the unit energy absorption and the octahedral shear strain was computed from the data in Step c by the use of Eq. 1.

Two specimens cut in the direction of rolling from each plate were tested, two from Plate No. 26 from Spec. No. 37 at a temperature of 76 Deg. F. and the two from Plate No. 4 for Spec. No. 38 at the temperature of -20 Deg. F. Because the true stress-strain curves in the directions parallel and transverse to the rolling direction were for all practical purposes identical, the calibration data in the direction of rolling was applied to the strains in the transverse direction in the large plates with openings.

## 2. Determination of Poisson's Ratio and the Tangent Modulus

The values of Poisson's ratio in Figs. 8 and 9 in the directions parallel and transverse to the rolling direction were required for the computation of the true stresses. The data from Step a above gave these values for the specimens in the direction of rolling. Two additional tensile specimens of the type in Fig. 2 were cut from each plate transverse to the direction of rolling and tested.

The following values of Poisson's ratio were found experimentally:

| Plate No. | Testing Temperature--Deg. F. | Poisson's Ratio in Direction Parallel to Rolling | Poisson's Ratio in Direction Transverse to Rolling | Use Values for Spec. No. |
|-----------|------------------------------|--|--|--------------------------|
| 26        | 76                           | 0.48   | 0.46   | 37                       |
| 4         | -20                          | 0.51   | 0.46   | 38                       |

Deviations from the theoretical value of 0.5 of the experimentally determined value occurred because of experimental errors and anisotropy of the material resulting from rolling.

#### VII. PILOT TEST AT LOW TEMPERATURE OF PLATE WITH SQUARE OPENING WITH ROUNDED CORNERS

While the transition temperature of the 1/2-in. plate material had been determined by the Navy tear test, it was unknown for the large plates with a square opening with rounded corners. Therefore, a pilot test was made on Spec. No. 38A at a temperature of zero Deg. F. and resulted in a fracture which was 87 per cent cleavage. A shear fracture started at the diagonally opposite corners of the opening, and after progressing a short distance, changed to a cleavage fracture. As a result of this test, it was decided that the testing temperature for Spec. No. 38 should be -20 Deg. F.

The load-average elongation curve for this specimen is shown in Fig. 11 and a photograph after fracture in Fig. 12.

#### VIII. TESTS OF TWO LARGE PLATES WITH SQUARE OPENING WITH ROUNDED CORNERS

##### 1. Tests and Type of Fracture.

Spec. No. 37 was tested at a temperature of 76 Deg. F. and Spec. No. 38 at -20 Deg. The fracture of the former was entirely shear,

while for the latter it was 91 per cent cleavage. Photographs of these plates after failure are shown in Fig. 12. The load-average elongation curves in Fig. 11 indicate that the over-all behavior of Spec. No. 38 at a temperature of -20 Deg. and of Spec. No. 38A at zero Deg. was essentially identical and that both underwent more elongation to ultimate load than Spec. No. 37 and almost as much elongation to failure. The predominantly cleavage fracture in the two low-temperature tests was initiated by a small portion of shear fracture. The probable explanation for this behavior may be that the stress-raising effect of the 1-1/8 in. radius at the corner of the opening was not sufficiently severe to initiate a cleavage fracture at a temperature of -20 Deg., but the crack which formed as failure began was.

## 2. Computation of the Unit Strain Energy Distribution by the Octahedral Theory

A brief description of the octahedral theory for computing the unit energy absorption in the plastic range of the material was presented in a previous section of this report. The elongation readings from the slide-wire resistance gages on Specs. No. 37 and 38 and the unit energy absorption in the calibration tensile tests were applied in the following manner to determine the unit energy absorption at various points in the large plates with openings:

1. From the elongation readings on the surface of Specs. No. 37 and 38, the natural strain values,  $E_x$  and  $E_y$ , were computed for each gage length.

2. Equation 5 was used to transform these natural strain values into the form of octahedral shear strains.
3. For each value of the octahedral shear strain found in Step 2, the corresponding unit strain energy absorption was read from Fig. 7.
4. The values from Step 3 were plotted on the surface of the specimens and unit strain energy contours drawn.
5. The volume under the surface representing the unit strain energy absorption at various points was equal to the total energy absorption within the gaged area and was compared with the energy absorption found for the same region from the load-average elongation curve in Fig. 11.

The unit strain energy contour maps for Spec. No. 37 at different loads are shown in Figs. 13 to 16, inclusive, and for Spec. No. 38 in Figs. 17 to 22, inclusive. The following observations may be made concerning the contour plots in these figures:

1. The pattern of the unit energy distribution which developed at the lower loads in the plastic range, changed somewhat as the ultimate load was approached. At the lower loads, the highest unit energy absorption was found at the corners of the opening and in the two regions extending diagonally upwards from the corners of the opening to the outer edge of the plates. At the highest loads, the largest unit energy absorption took place at the corners and along the vertical edges of the opening and in the regions immediately to the

right and the left of the opening which are adjacent to the transverse centerline of the plate.

2. At the lower loads in the plastic range, the unit energy absorption was highest in the regions where elastic stress theory would predict the highest values of the principal tensile stress. At the higher loads, the unit energy absorption was highest in the region of the least cross-section area.
3. The highest unit energy absorption was found at the tangent point between the corner arc and the vertical side of the opening, the point where elastic stress theory would predict the maximum elastic principal tensile stress. The maximum value at this point was 18,300 in-lb per cu in for Spec. No. 37 and 20,000 in-lb per cu in for Spec. No. 38. These maximum values should not be taken as the absolute maximum for the specimens, because they represent the average value within a one-inch gage length adjacent to the edge of the opening.
4. Fracture began at the tangent point where the maximum energy absorption was observed.

When the unit energy values on the contour maps in Figs. 13 to 22, inclusive, were integrated, the total energy absorbed within the gaged area was determined and compared with the total energy absorption computed from the load-average elongation curves in Fig. 11. The following table gives the results of this comparison:

| Refer to<br>Fig. No.                              | Load Lb. | Total Energy Absorption in In-Lb. |                                       |
|---|----------|-----------------------------------|---------------------------------------|
|   |          | From Octahedral<br>Theory         | From Load-Average<br>Elongation Curve |
| <u>Spec. No. 37 at Temperature of 76 Deg. F.</u>  |          |                                   |                                       |
| 13  | 500,000  | 79,400                            | 60,600                                |
| 14  | 650,000  | 243,000                           | 270,000                               |
| 15  | 720,000  | 426,000                           | 452,000                               |
| 16  | 800,000  | 1,056,000                         | 884,000                               |
| <u>Spec. No. 38 at Temperature of -20 Deg. F.</u> |          |                                   |                                       |
| 17  | 500,000  | 71,500                            | 21,000                                |
| 18  | 650,000  | 282,850                           | 225,000                               |
| 19  | 720,000  | 444,450                           | 370,000                               |
| 20  | 800,000  | 683,800                           | 638,000                               |
| 21  | 870,000  | 1,103,800                         | 1,021,000                             |
| 22  | 915,000  | 1,450,150                         | 1,389,000                             |

An examination of these values indicates that the agreement between the values of the energy absorption was better at intermediate and high loads than at low loads. At the lowest load of 500,000 lb. many of the elongation readings were of about the same magnitude as the sensitivity of the slide-wire resistance gages.

### 3. Rate of Increase of Unit Energy Absorption.

The manner in which the total energy absorption increased as the applied load increased is given in Fig. 23. At the same load, the total energy absorption was almost the same for Specs. No. 37 and 38, although the former was tested at 76 Deg. F. and the latter at -20 Deg. F.



However, the total energy to ultimate load was greater for Spec. No. 38, since it reached a higher ultimate load.

The plots of the unit strain energy contours for Specs. No. 37 and 38, as shown in Figs. 13 to 22, indicated that the unit energy absorption increased more rapidly in some portions of the specimens than in others, as the applied load was increased. The manner of this increase was analyzed to determine whether it followed any consistent pattern for any one specimen and whether the behavior of the two plates was in any way similar.

The unit energy absorption  $U$  at each point on the specimen was plotted against the applied load  $P$ . The upper diagrams in Fig. 24 show typical examples of the plots made at every one of the 124 points on each specimen as well as the plot of the average unit energy absorption for the whole specimen. It was found that the relation between the logarithm of the unit energy absorption and the applied load could be expressed empirically in a linear manner as shown in the lower diagrams of Fig. 24. The general equation of these semi-logarithmic plots was of the form,

$$U = e^{A+BP} \quad (14)$$

where  $A$  determines the intercept of the curve on the unit strain energy axis,  $B$  expresses the rate at which the unit strain energy increases, and  $P$  is the applied load. It was observed in these tests that there was an insignificant variation of the value of  $A$  in the many plots and that the exponent  $B$  largely determined the magnitude of the unit energy value. Accordingly, the rate at which the unit strain energy increased at the

various points on the specimen was analyzed by computing the value of the exponent B.

Since the exponent B is the slope of the semi-logarithmic plot, a comparison of the rates of increase of the unit strain energy at the different points was made by comparing these slopes. When the slope of the average unit strain energy absorption for the whole specimen was termed  $B_{av}$  and the slope at any point "n" as  $B_n$ , the ratio,  $B_n/B_{av}$  expressed the relative rate of unit strain energy increase. This relative rate of increase was computed for all points. Figs. 25 and 26 show contour lines connecting the points at which the values of the ratio  $B_n/B_{av}$  were equal. Where the rate of increase was equal to, or greater than the average value, the contours are full lines. Where the rate was smaller, the contours are dashed lines.

The unit strain energy increased most rapidly in the trapezoidal-shaped area on either side of the opening in the two specimens, that is, in the region of the least cross-section area. The unit strain energy increased less rapidly than the average value for the whole specimen in the region above the opening. The greatest rate of increase was found at the corners of the opening and the least rate in the area just above the opening close to the vertical centerline of the specimen.

Fig. 23 indicates that the total energy absorption was almost the same at the same loads for Specs. No. 37 and 38. Since these were identical specimens, the unit strain energy absorption for the two was essentially equal. Therefore, when the plot of the rate of increase of unit strain energy in Fig. 25 is compared with that of Fig. 26, the values in one diagram may be considered to be directly relative to those in the other. A comparison of the contours in these two figures reveals the following points of interest:

1. The areas of high and low values were more spread out in the case of Spec. No. 37 tested at 76 Deg. F. than in Spec. No. 38 tested at -20 Deg. F. The area in which the values of the rate of increase were greater than unity was 46 per cent of the gaged area in the former specimen and 36 per cent in the latter.

2. The values of the rate of increase varied from 0.71 to 1.30 for the room-temperature test and from 0.59 to 1.27 for the low-temperature test. While the maximum rate of increase was almost equal for the two tests, the range of variation was greater for the low-temperature specimen. The gradient of the rate of increase was steeper in the test at the lower temperature.

It must be remembered in comparing the numerical values of the contours in Figs. 25 and 26 that they are exponential values and that the variation from the minimum to the maximum value represents quite a large difference in the energy absorption.

4. Computation of the True Stress Distribution on Transverse Cross-Sections at the Ultimate Load.

The true stresses at ultimate load on the same four transverse cross-sections of Specs. No. 37 and 38 were computed by the use of Eqs. 12 and 13 in Section IV of this report and the data of the true stress-strain curves presented in Figs. 6, 8, 9, and 10. The true stress distribution in the axial, or vertical direction of the specimen computed on these four cross-sections is shown for Spec. No. 37 in Figs. 27 to 30, inclusive, and for Spec. No. 38 in Figs. 31 to 34, inclusive. The actual or true

thickness of the plate and the force per lineal inch of the actual plate width are given in these figures also.

If these stress distributions are examined in a general way, it may be seen that their pattern was similar to that which would occur under elastic stresses. The stress distribution in the region of the opening was non-uniform with the highest values of the tension stress near the corner. On cross-sections more remote from the opening, the stress distribution became more nearly uniform, but was still far from uniform. Low tensile stresses or even compression stresses were present in the area just above the opening. The pattern of the stress distribution in Specs. No. 37 and 38 was much the same, but the values of the true stresses in the latter were higher than in the former specimen because of the higher load which was being applied.

The correctness of the individual stress values can be surmised only intuitively. In the calibration tensile tests, the average true stress at which necking began was 75,500 psi in the tests at 76 Deg. F. and 81,600 psi in the tests at -20 Deg. F. The average true stress at fracture was 122,500 psi in the former tests and 115,400 psi in the latter. The true stresses plotted in Figs. 27 to 34 were of the same order of magnitude as these true stresses found in the calibration tensile tests. Their magnitudes were also such as might be expected in a notched plate at its ultimate load.

It is interesting that the maximum values of the true tensile stress occurred in the regions where the greatest unit energy absorption was found. The fracture in both specimens was initiated in the

corner of the opening where the highest values of the energy absorption and the true stress appeared.

An indirect method of checking these true stress values is to sum up the stresses on different transverse cross-sections of the specimen to obtain the total applied force. A comparison of the values of the total load found by integrating the upper curve in Figs. 27 to 34, the diagram which shows the force per lineal inch of plate width, with the actual testing machine load at ultimate load is as follows:

Cross-Section                      Computed Total Load-lb.

Spec. No. 37 at Temperature of 76 Deg. F.  
Load of 800,000 lb.

|     |         |
|-----|---------|
| a-a | 894,000 |
| b-b | 750,000 |
| c-c | 784,000 |
| d-d | 720,000 |

Spec. No. 38 at Temperature of -20 Deg. F.  
Load of 915,000 lb.

|     |           |
|-----|-----------|
| a-a | 1,060,000 |
| b-b | 1,126,000 |
| c-c | 1,100,000 |
| d-d | 1,032,000 |

Reasonably good correlation was found between the values of the total load derives from the computed values of the true stresses and the actual testing machine load.

## IX. SUMMARY AND CONCLUSIONS

Two methods of analysis of plastic flow, the octahedral theory for computing the unit energy absorption and a method developed in the course of this investigation for computing true stresses, were applied in the case of two large plates with square openings with rounded corners. The first failed with a completely shear fracture at a temperature of 76 Deg. F. and the second with a fracture 91 per cent cleavage at a temperature of -20 Deg. F. Both methods of analysis utilized the experimental strain data from these tests.

From the limited application of the octahedral theory made in this investigation, it was found that this method of analysis gave unit energy distributions, which, when integrated, produced values of the total energy absorption which agreed fairly closely with the energy absorption determined from the load-average elongation curve. This method presents a dependable, though laborious means of studying plastic flow and fracture in structural members. These conclusions are essentially those which resulted from an earlier application of the method.<sup>3</sup>

The two specimens absorbed approximately the same amounts of energy at the same loads up to the ultimate load, although one failed with a completely shear fracture and the other with a fracture almost completely cleavage. However, the gradient of the rate of increase of the unit strain energy was steeper in the latter than in

---

<sup>3</sup> Ibid, page 2

the former and the greater part of the total energy was absorbed in a smaller portion of the specimen.

The method of computing true stresses in the plastic range of the material was applied for the first time and gave results which correlated reasonably well with the observed data. It was found to be less laborious than the procedure required for computing elastic stresses from observed elastic strains. The method would not work well in the so-called "flat" portion of the stress-strain curve and, at stresses in the range where necking of the material is occurring, would be subject to some interpretation, since Poisson's ratio has an anomalous meaning, if applied in this range. Further applications of the method are required to test its reliability.

The use of the slide-wire resistance gages for measuring elongations permitted the tests to be made continuously and in a period of time short enough to reduce strain-aging of the specimen to a negligible amount.

X. SYMBOLS

- U Unit strain energy, in-lbs. per cu. in.
- $\tau$  Octahedral shear stress, psi.
- $\gamma$  Octahedral shear strain.
- X, Y Coordinate axes, the rolling direction and the applied tensile force are parallel to the y-axis.
- Z Coordinate axis perpendicular to the plate.
- $\sigma_x, \sigma_y, \sigma_z$  True stresses, psi.
- $\epsilon_x, \epsilon_y, \epsilon_z$  Natural strains.
- $\bar{\sigma}_x, \bar{\sigma}_y, \bar{\sigma}_z$  True stresses from an experimental true stress-strain diagram, psi.
- $\bar{\epsilon}_x, \bar{\epsilon}_y, \bar{\epsilon}_z$  Natural strains from an experimental true stress-strain diagram.
- $E_{Tx}, E_{Ty}$  Tangent moduli as determined from the true stress-strain diagram in the x- and y-direction, psi.
- $\beta_x, \beta_y$  Intercepts of the tangent to the true stress-strain diagram on the natural strain axis.
- $\mu_{xy}, \mu_{yx}$  Poisson's ratio in this report is interpreted in terms of natural strains.

$$\mu_{xy} = \frac{\epsilon_y}{\epsilon_x}$$

- e Base of the natural logarithm.
- P Applied axial force, kips.
- A Intercept on the u-axis of a semi-logarithmic plot of u against the applied force P.
- B Slope of a semi-logarithmic plot of u against the applied force P.



## XI. ACKNOWLEDGMENTS

The investigation reported herein was sponsored by the Ship Structure Committee and was carried out in the Structural Research Laboratory of the Department of Civil Engineering, University of Washington, of which Professor R. B. Van Horn is head, and in the College of Engineering, of which Dr. H. E. Wessman is dean. The test program and the preparation of the report were under the direction of Dr. R. A. Hechtman, Associate Professor of Structural Research. Dr. D. Vasarhelyi was project engineer and was assisted by Mr. K. J. Kenworthy and Mr. Y. T. Yoshimi, graduate research fellows, and Mr. R. B. Matthieson, computer and draftsman. Included in this report are two theses<sup>4,5</sup> prepared in partial fulfillment of the degree of Master of Science in Civil Engineering.

The authors wish to express their appreciation to Mr. John Vasta of the Bureau of Ships, Department of the Navy, Dr. Finn Jonassen of the National Research Council, and Professor F. B. Farquharson, Director, Engineering Experiment Station, University of Washington, for their suggestions and encouragement.

---

<sup>4</sup> K. J. Kenworthy, A Determination of Strain Energy Distribution and True Stresses in the Plastic Range in Plates with Openings, Thesis, University of Washington, 1951.

<sup>5</sup> Y. T. Yoshimi, Unfinished thesis, University of Washington, 1951.

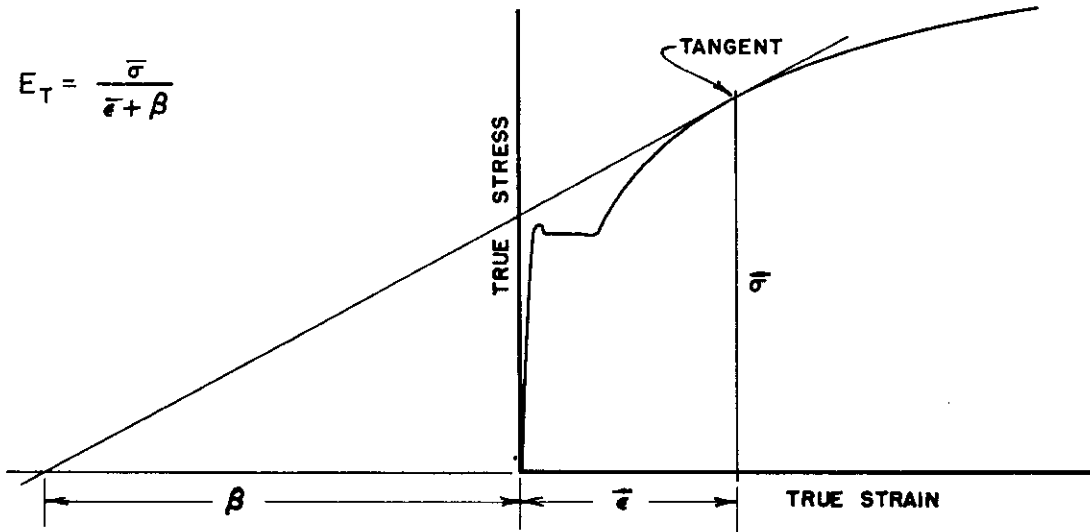
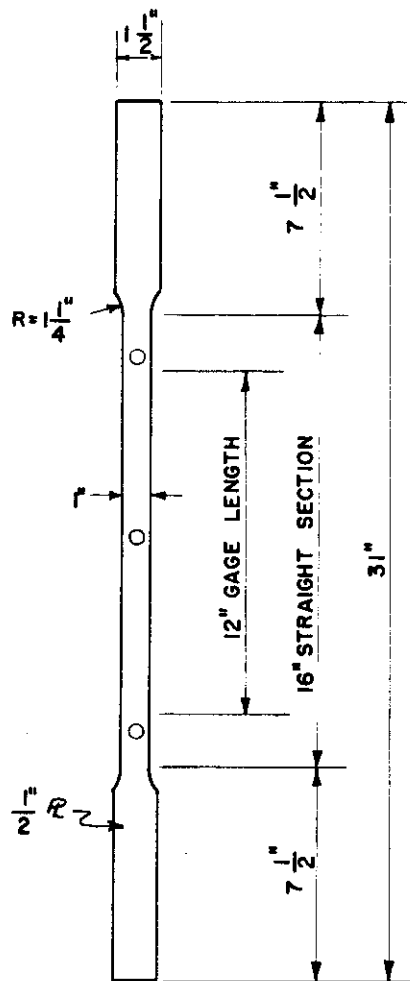
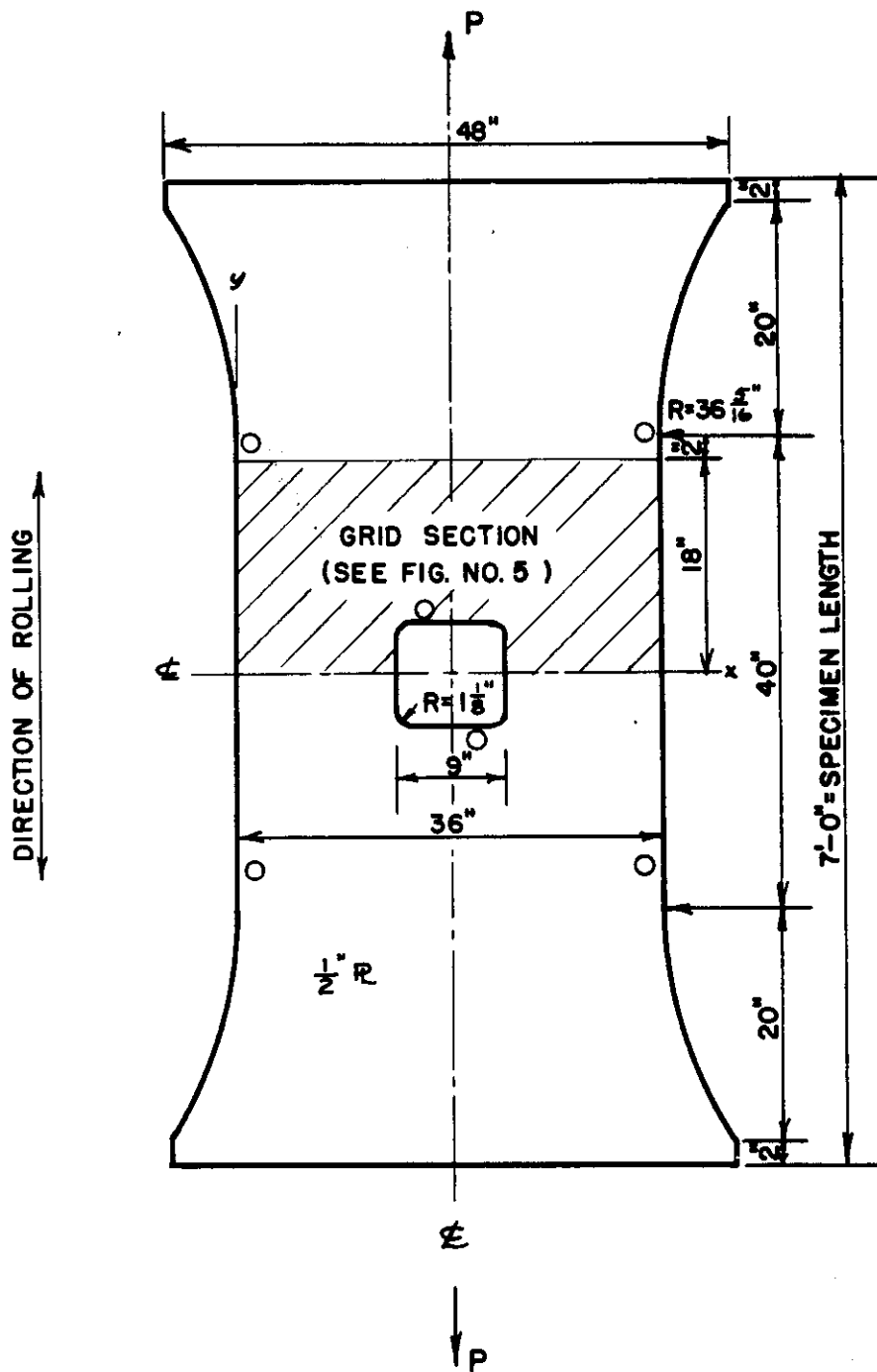


Fig. 1 . Graphical Definition of  $E_T$  and  $\beta$  .



○ LOCATION OF THERMOCOUPLES

Fig. 2 . Sketch of Tensile Calibration Test Specimen.



○ LOCATION OF THERMOCOUPLES

Fig. 3 . Plate with Square Opening with Rounded Corners.

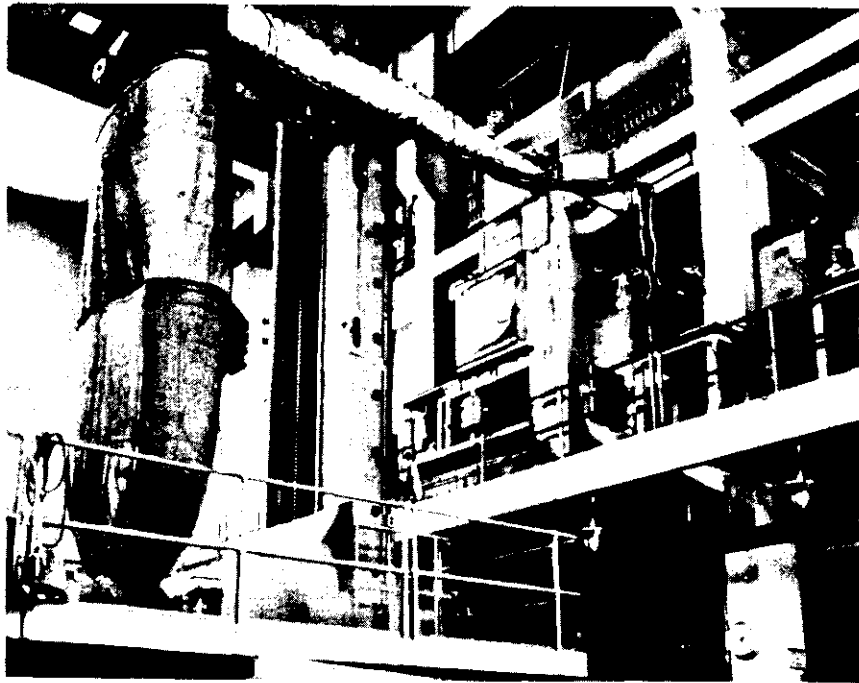


Fig. 4 Cooling Chamber Enclosing the Plate Specimen.

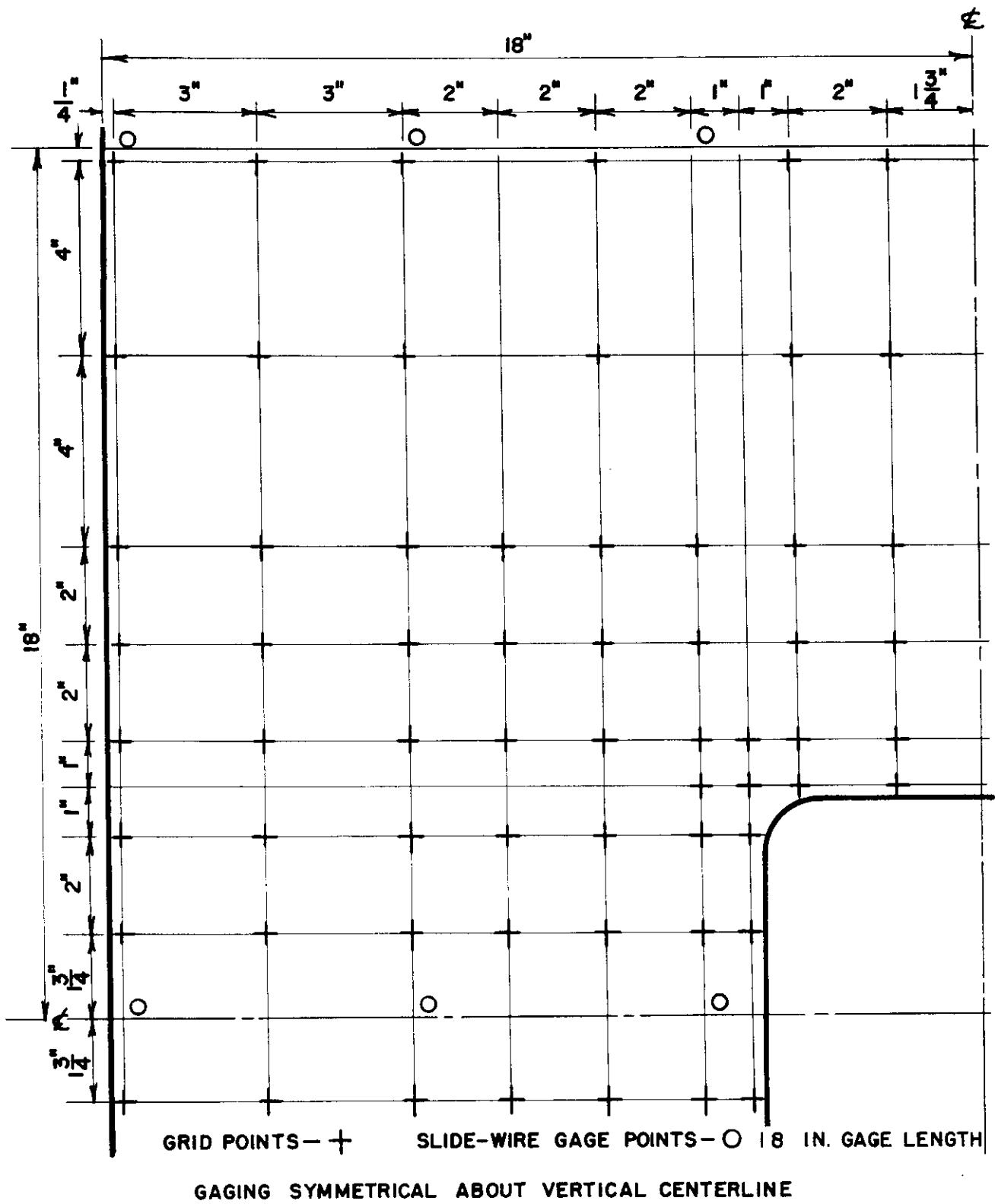


Fig. 5 . Location of Grid and Slide-Wire Gages.

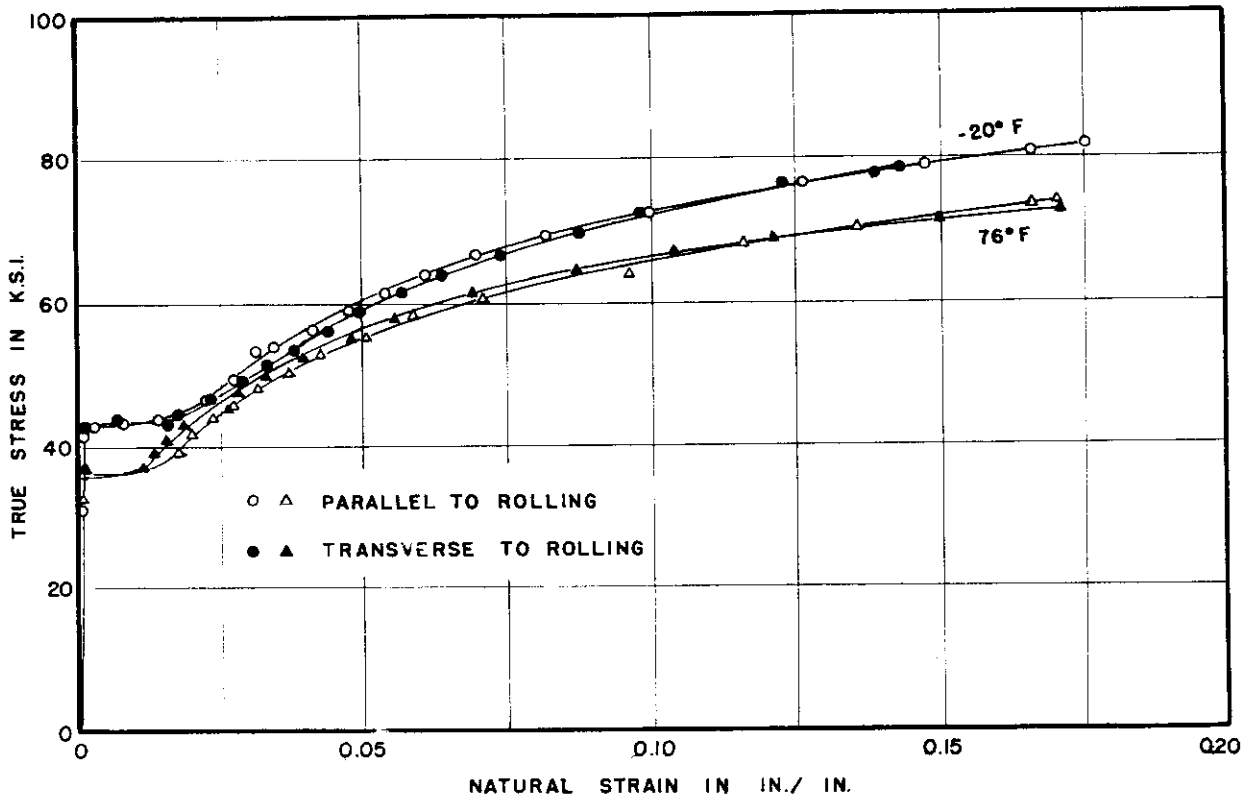


Fig. 6 Calibration Test True Stress-Strain Curves.

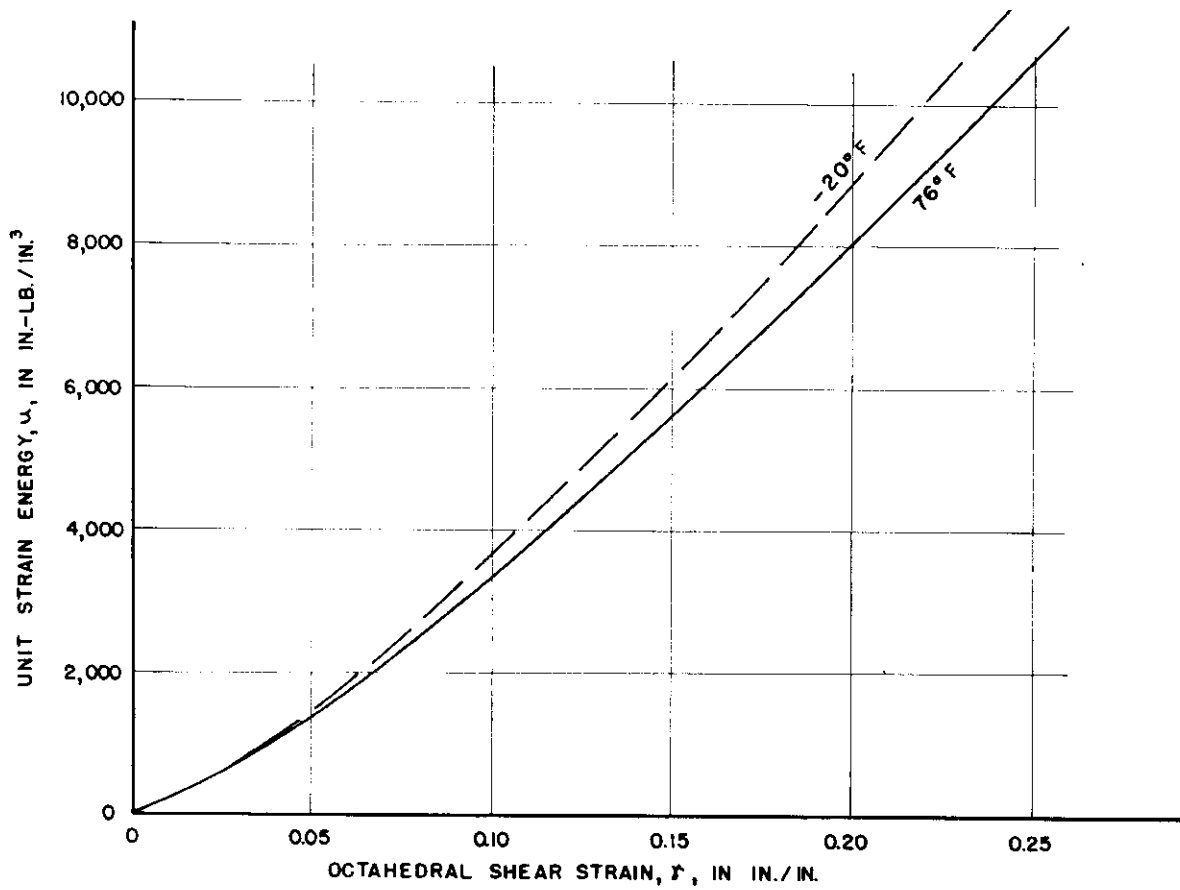


Fig. 7 Relation of Unit Strain Energy Absorption and Octahedral Shear Strain for Calibration Test Specimen.

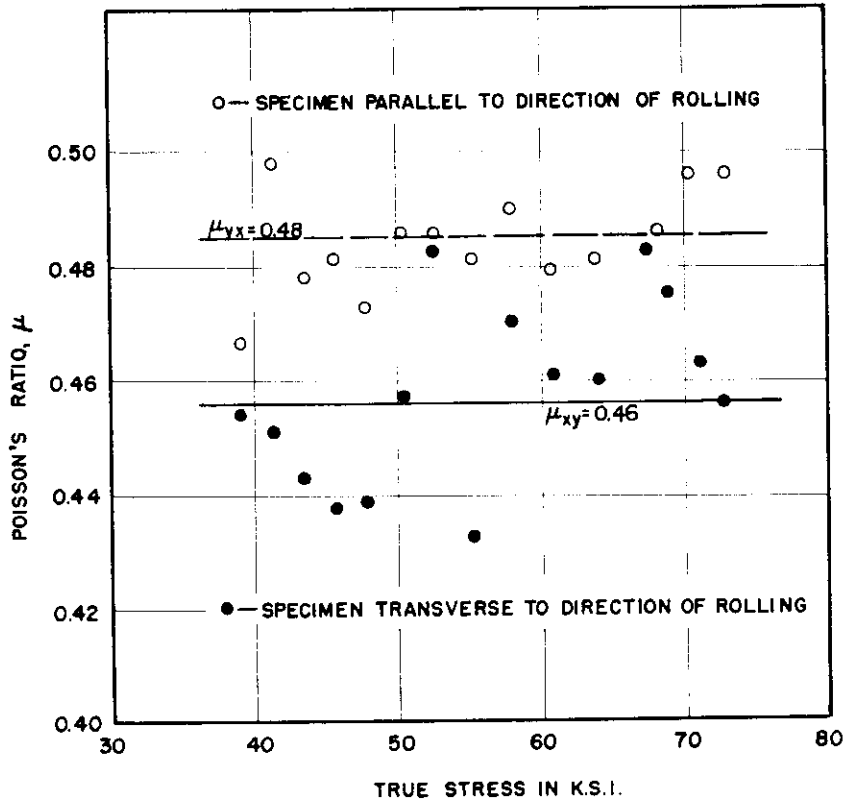


Fig. 8 . Plot of Poisson's Ratio as a Function of True Stress in Plastic Range of Calibration Test Specimen, 76 Deg. F.

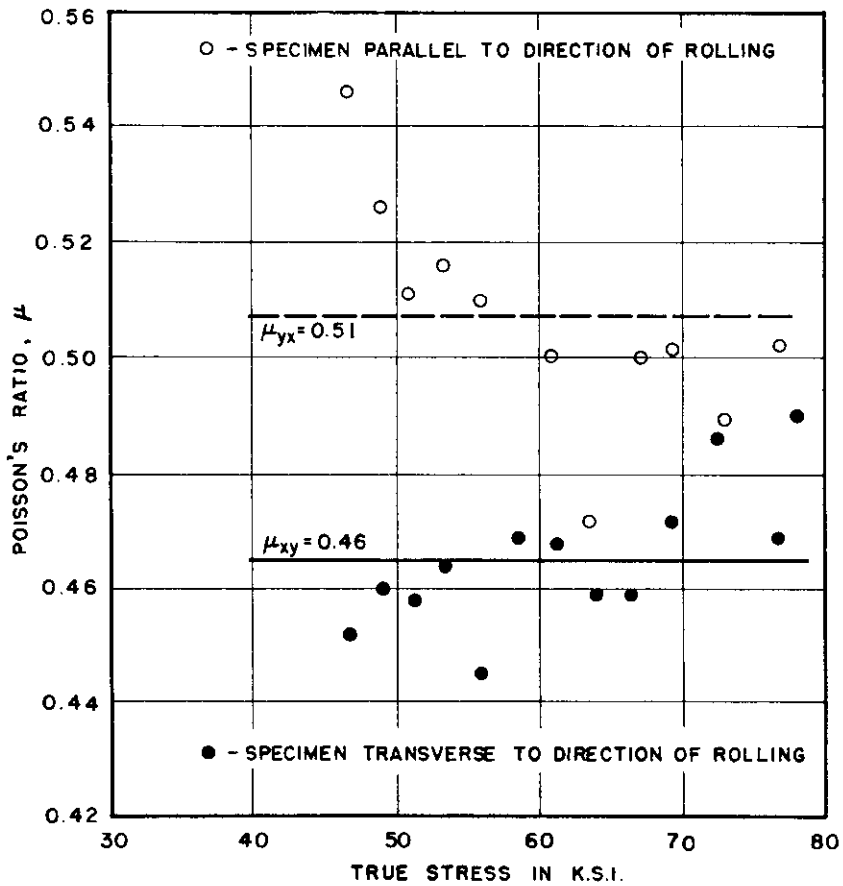


Fig. 9 Plot of Poisson's Ratio as a Function of True Stress in Plastic Range of Calibration Test Specimen, -20 Deg. F.

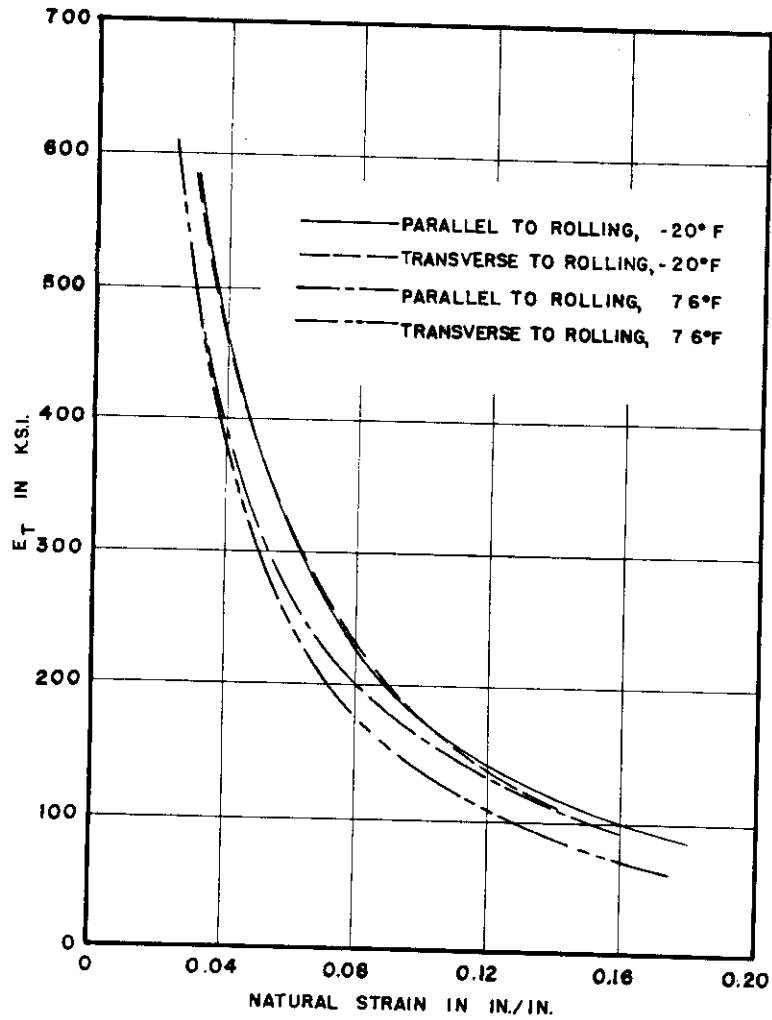


Fig. 10 Plot of  $E_T$  as a Function of Natural Strain.

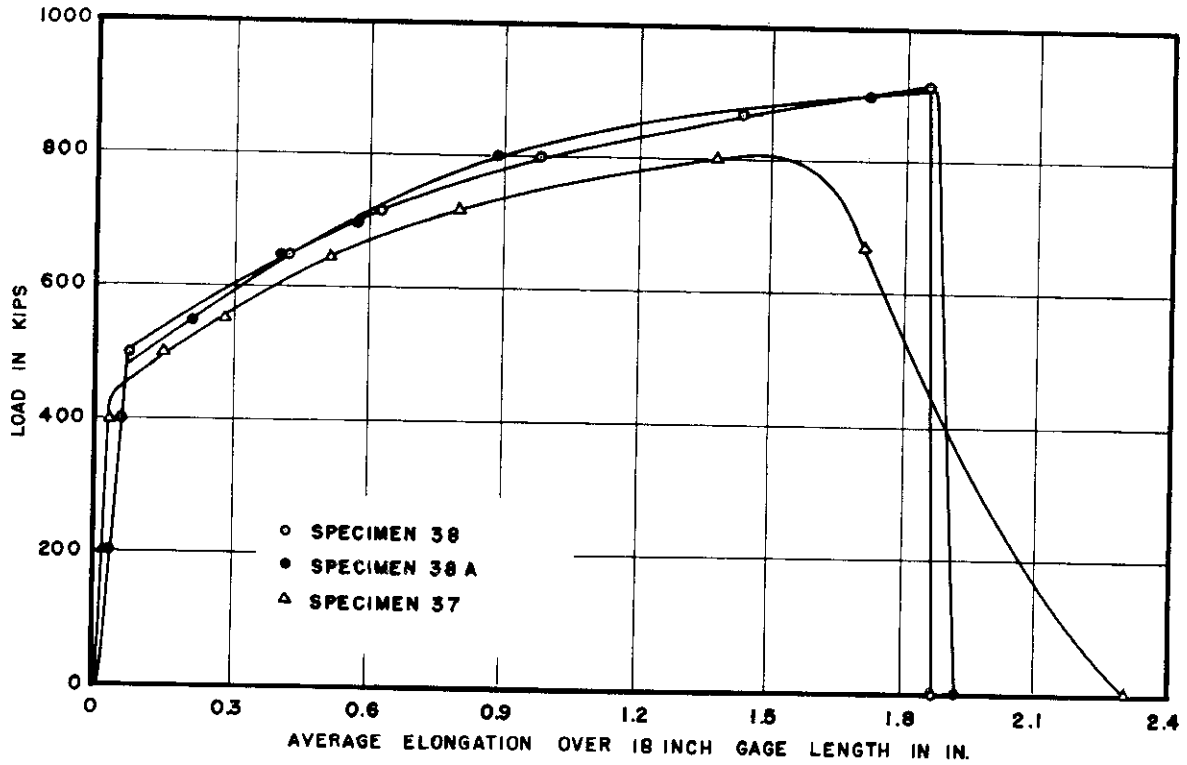
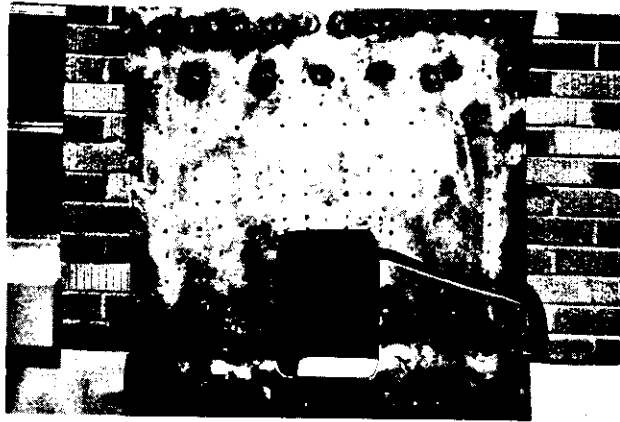
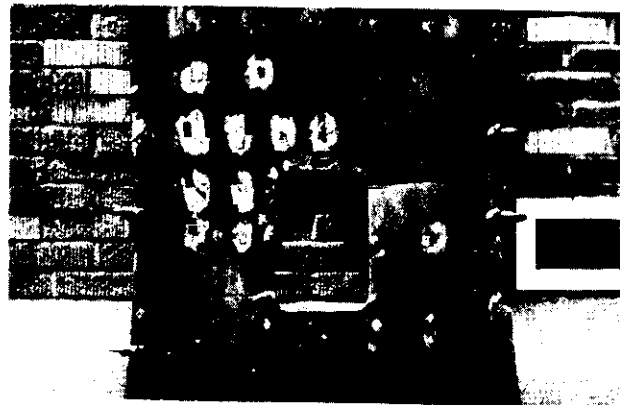


Fig. 11 Load-Average Elongation Curves for Plates with Square Opening with Rounded Corners.

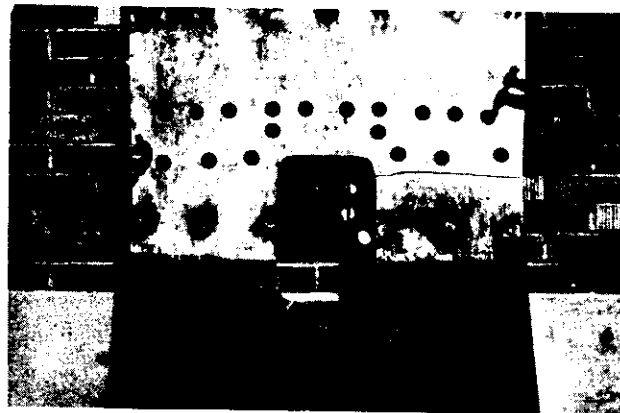




Spec. No. 37



Spec. No. 38/A



Spec. No. 38.

Fig. 12 Photographs of Plates after Failure.

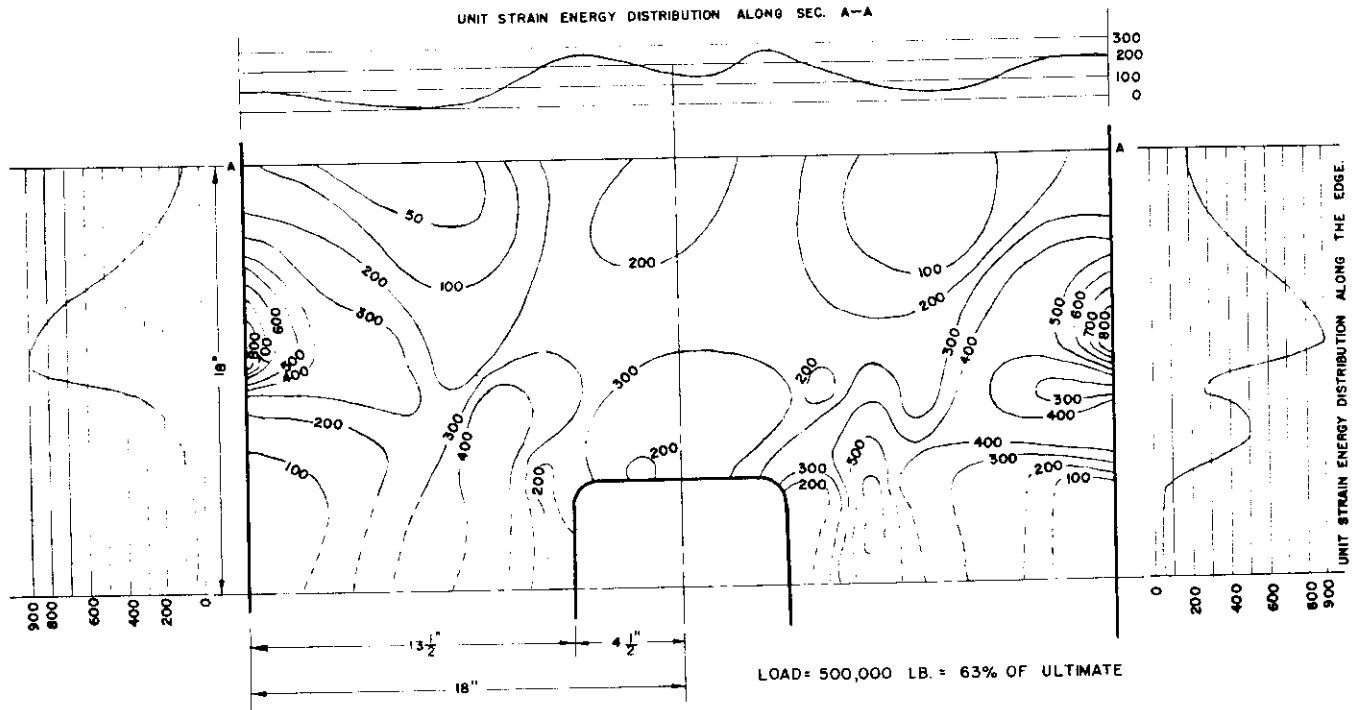


Fig. 13. Unit Strain Energy Contours for Plate with Square Opening with Rounded Corners for Load of 500 kips, 63 Per Cent of Maximum Load. Spec. No. 37. Temperature 76° F.

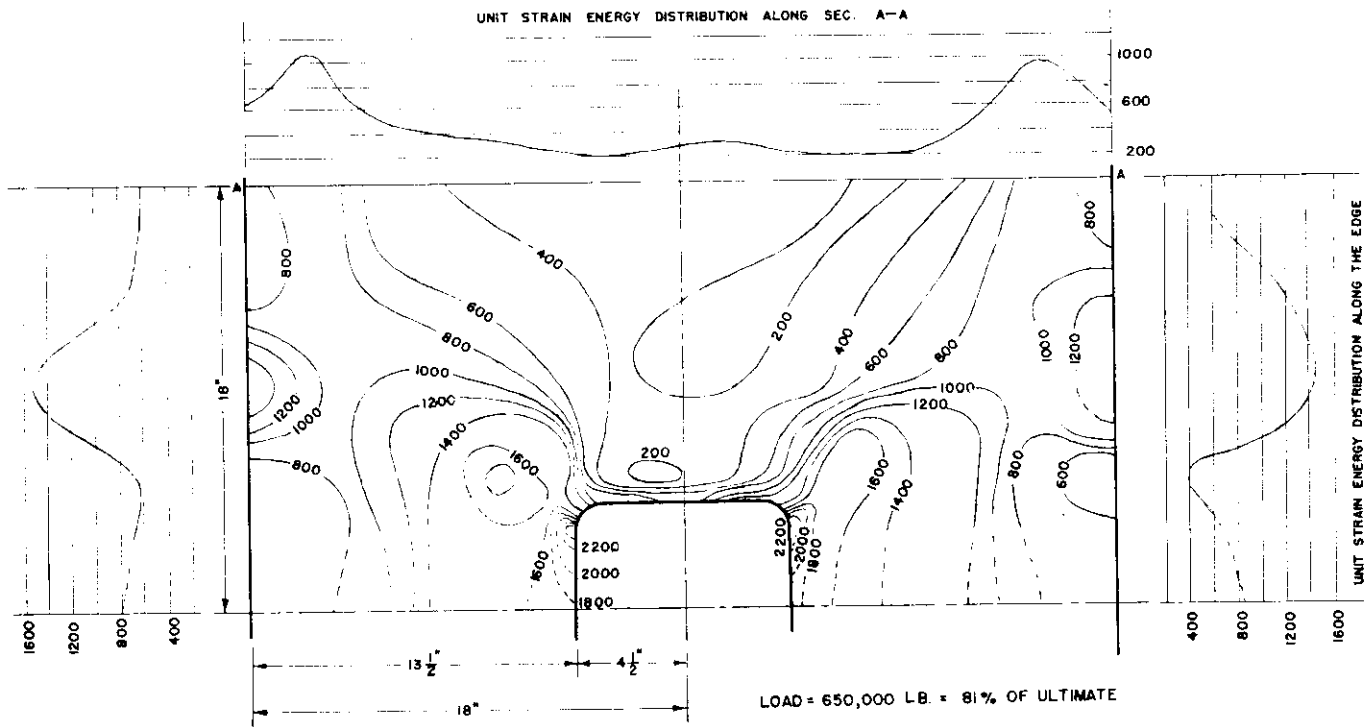


Fig. 14. Unit Strain Energy Contours for Plate with Square Opening with Rounded Corners for Load of 650 kips, 81 Per Cent of Maximum Load. Spec. No. 37. Temperature 76° F.

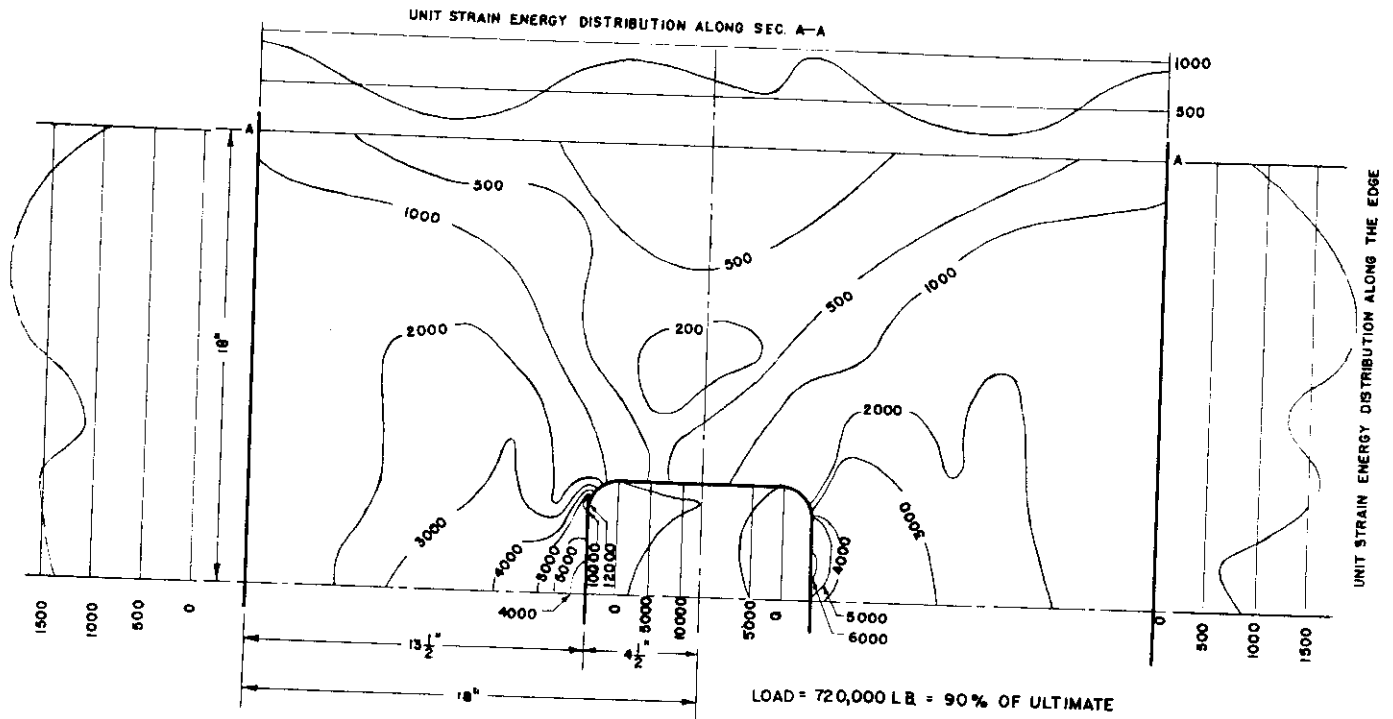


Fig. 15. Unit Strain Energy Contours for Plate with Square Opening with Rounded Corners for Load of 720 kips, 90 Per Cent of Maximum Load. Spec. No. 37. Temperature 76°F.

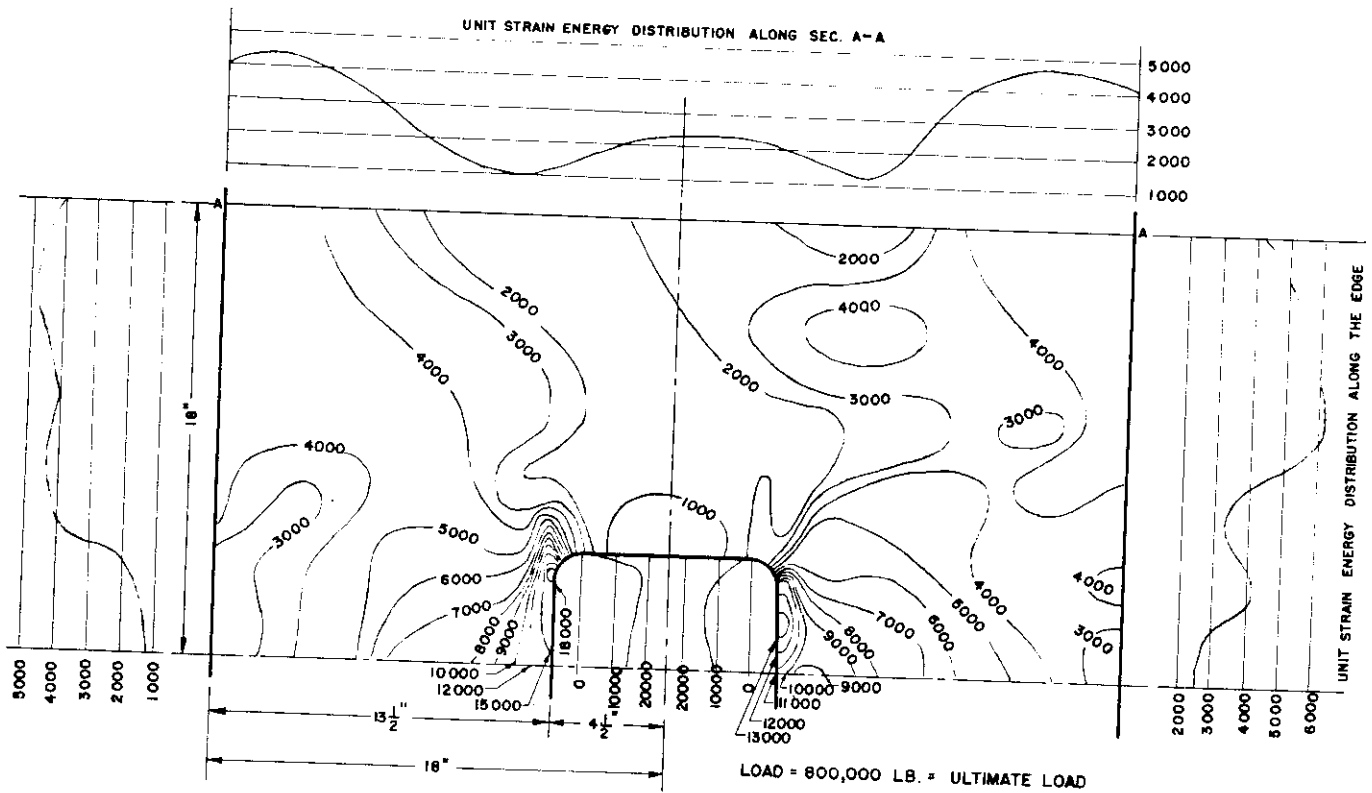


Fig. 16. Unit Strain Energy Contours for Plate with Square Opening with Rounded Corners for Load of 800 kips, 100 Per Cent of Maximum Load. Spec. No. 37. Temperature 76°F.

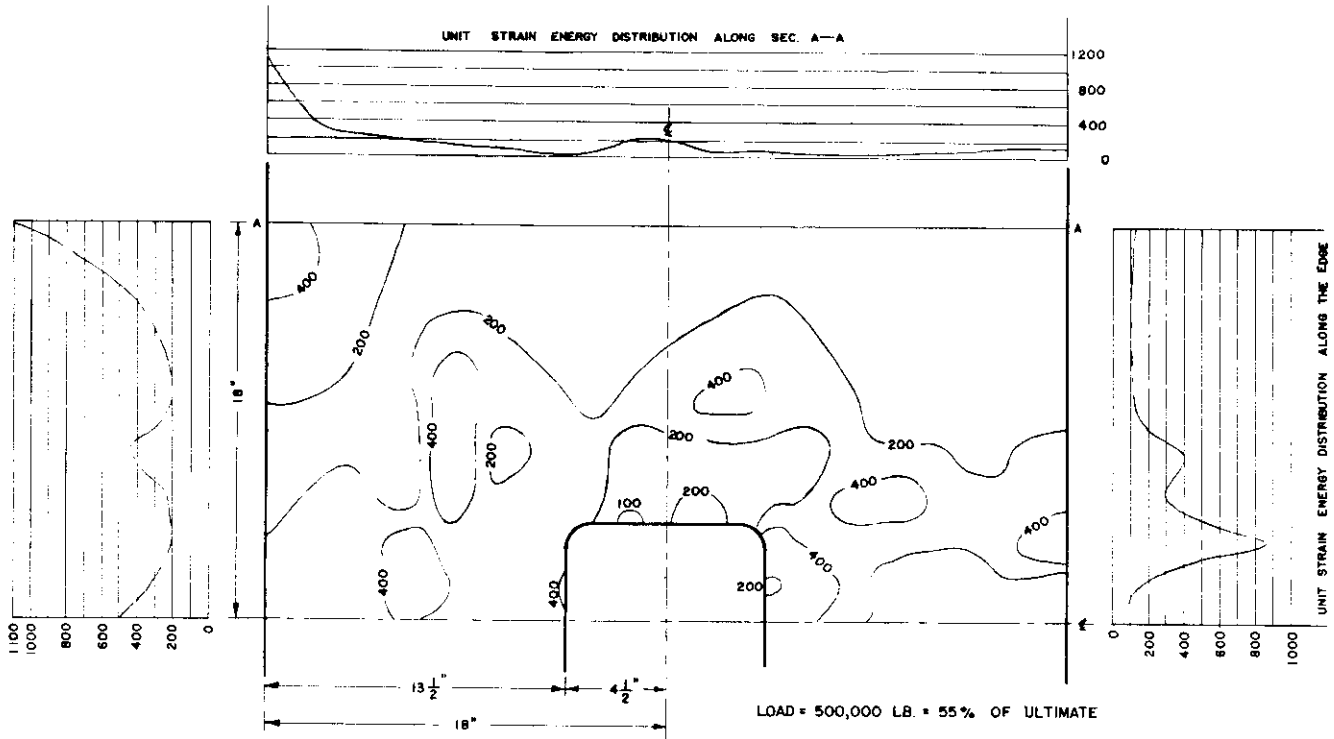


Fig. 17 Unit Strain Energy Contours for Plate with Square Opening with Rounded Corners for Load of 500 kips, 55 Per Cent of Maximum Load. Spec. No. 38. Temperature -20° F.

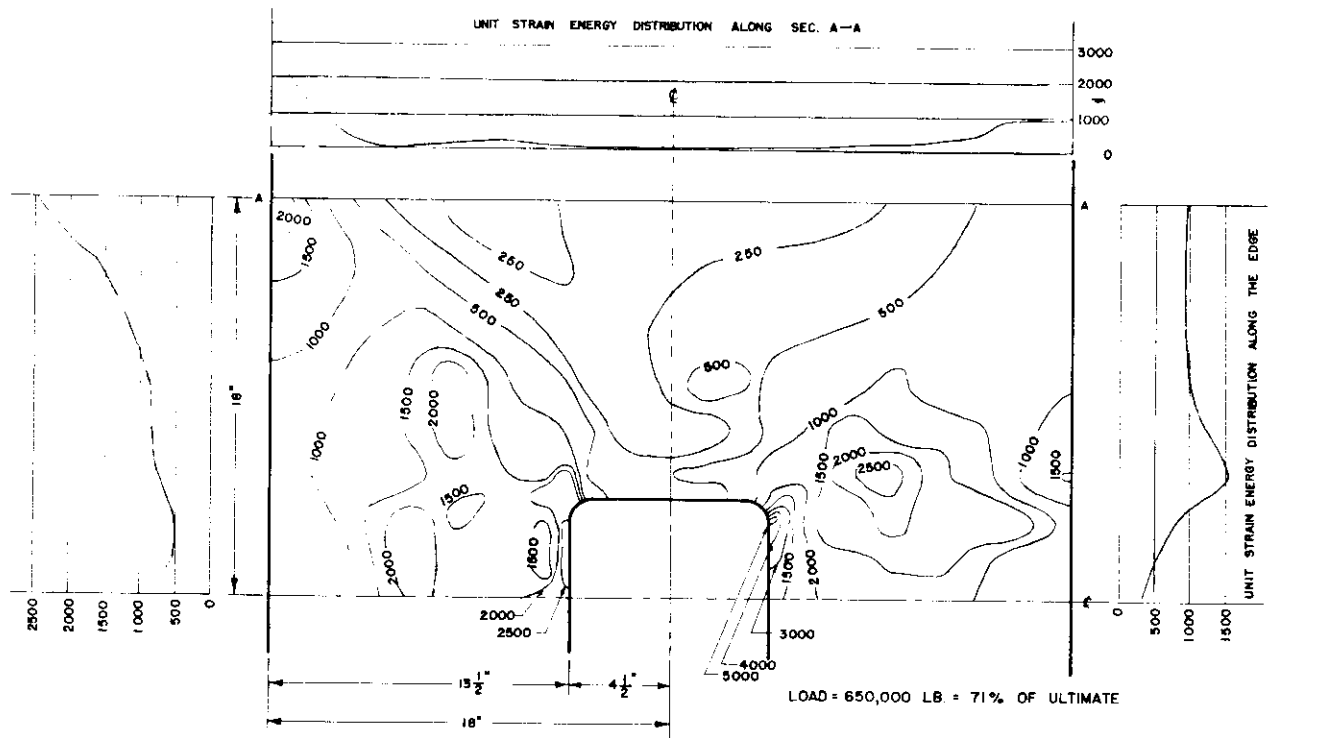


Fig. 18 Unit Strain Energy Contours for Plate with Square Opening with Rounded Corners for Load of 650 kips, 71-Per Cent of Maximum Load. Spec. No. 38. Temperature -20° F.

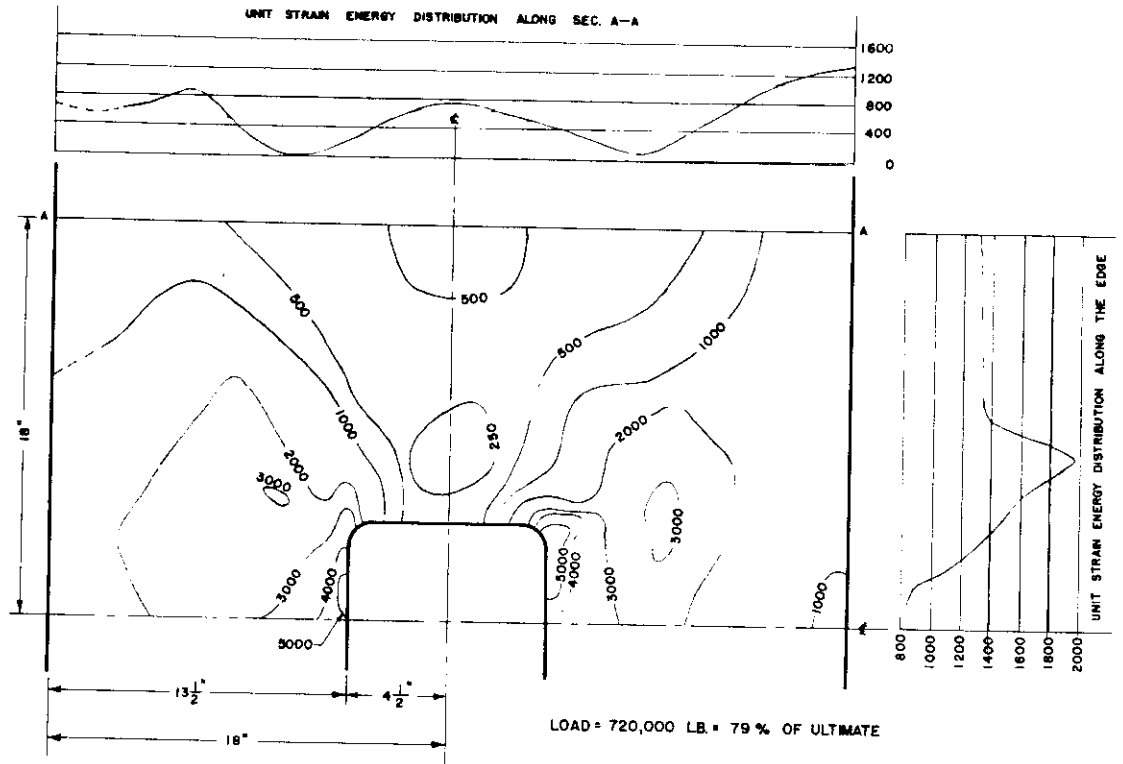


Fig. 19 Unit Strain Energy Contours for Plate with Square Opening with Rounded Corners for Load of 720 kips, 79 Per Cent of Maximum Load. Spec. No. 38. Temperature  $-20^{\circ}\text{F}$ .

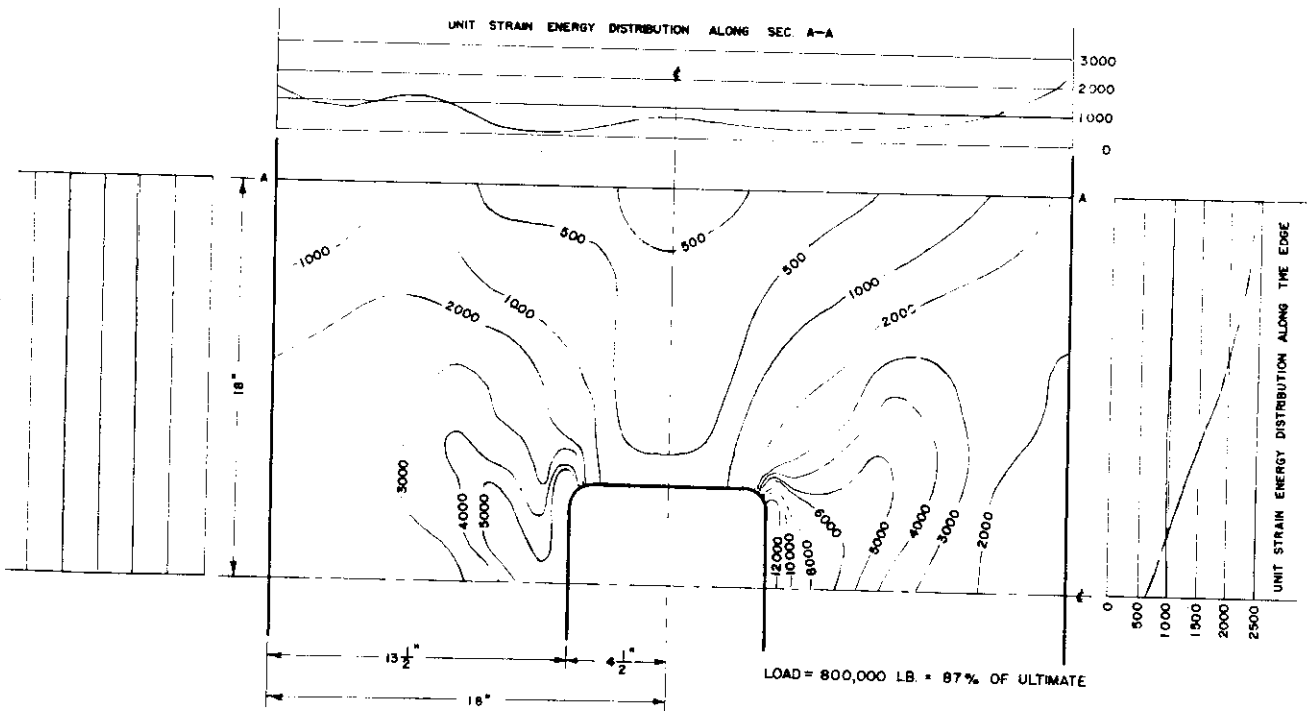


Fig. 20 Unit Strain Energy Contours for Plate with Square Opening with Rounded Corners for Load of 800 kips, 87 Per Cent of Maximum Load. Spec. No. 38. Temperature  $-20^{\circ}\text{F}$ .

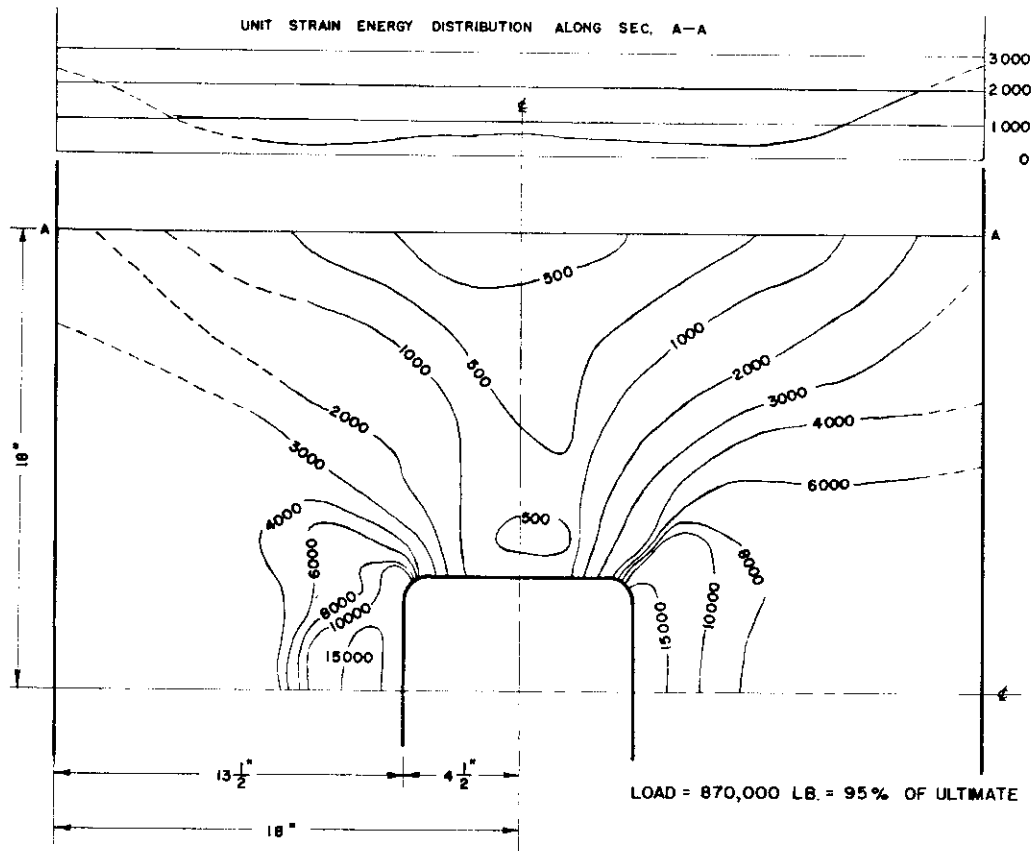


Fig. 2.1 Unit Strain Energy Contours for Plate with Square Opening with Rounded Corners for Load of 870 kips, 95 Per Cent of Maximum Load. Spec. No. 38. Temperature -20°F.

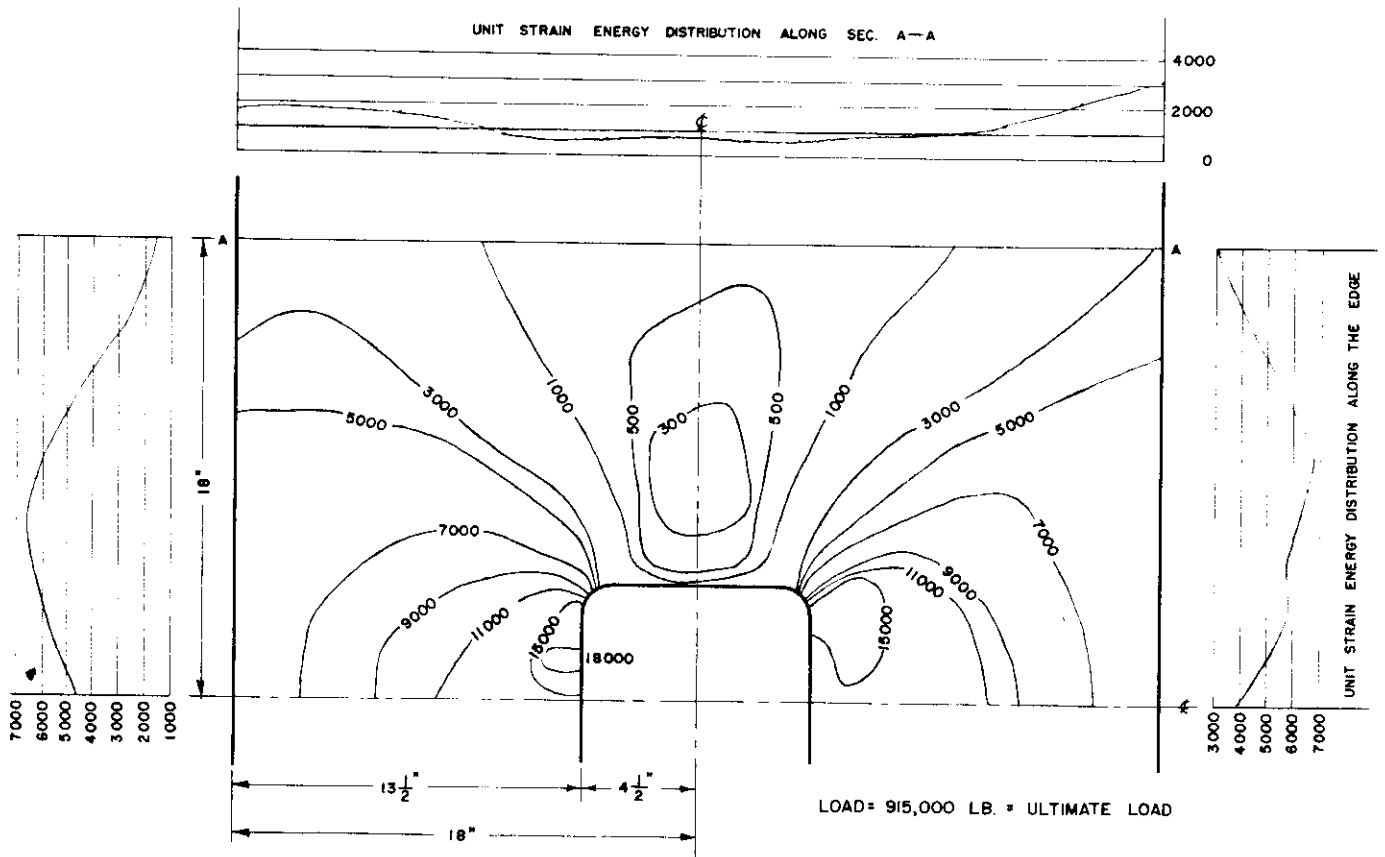


Fig. 2.2 Unit Strain Energy Contours for Plate with Square Opening with Rounded Corners for Load of 915 kips, 100 Per Cent of Maximum Load. Spec. No. 38. Temperature -20°F.

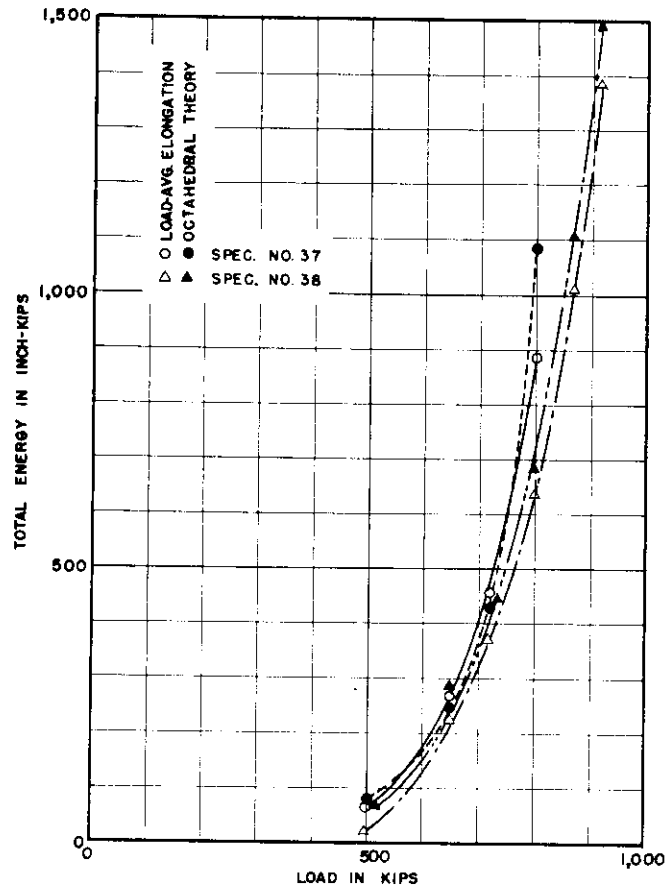


Fig. 23 Comparison of Total Strain Energy and Applied Load for Plates with Square Openings with Rounded Corners.

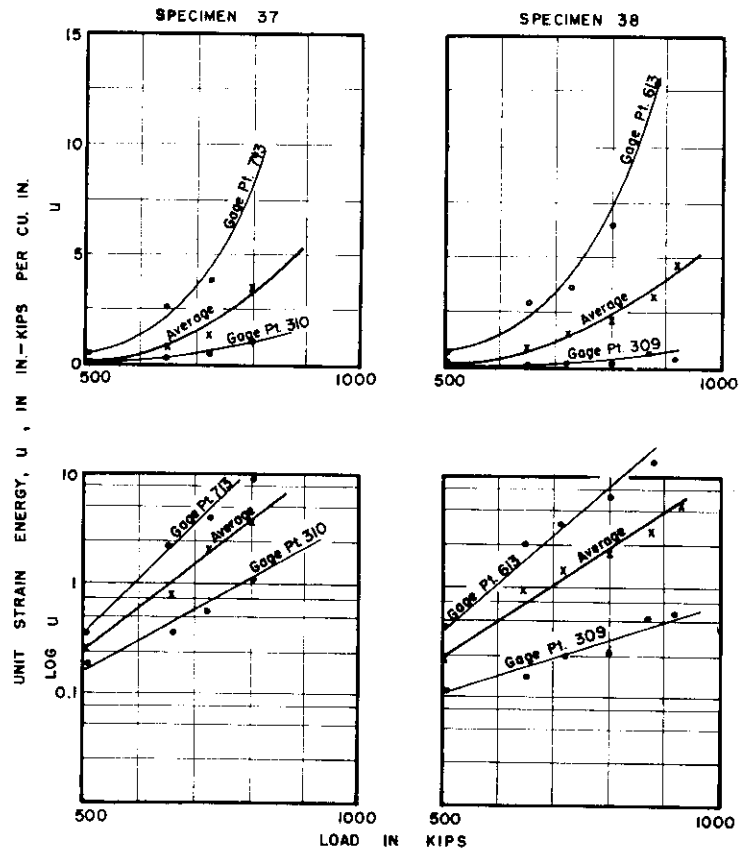


Fig. 24 Growth of Unit Strain Energy at Typical Points on Specimens Under Applied Load. Specs. No. 37 and 38.

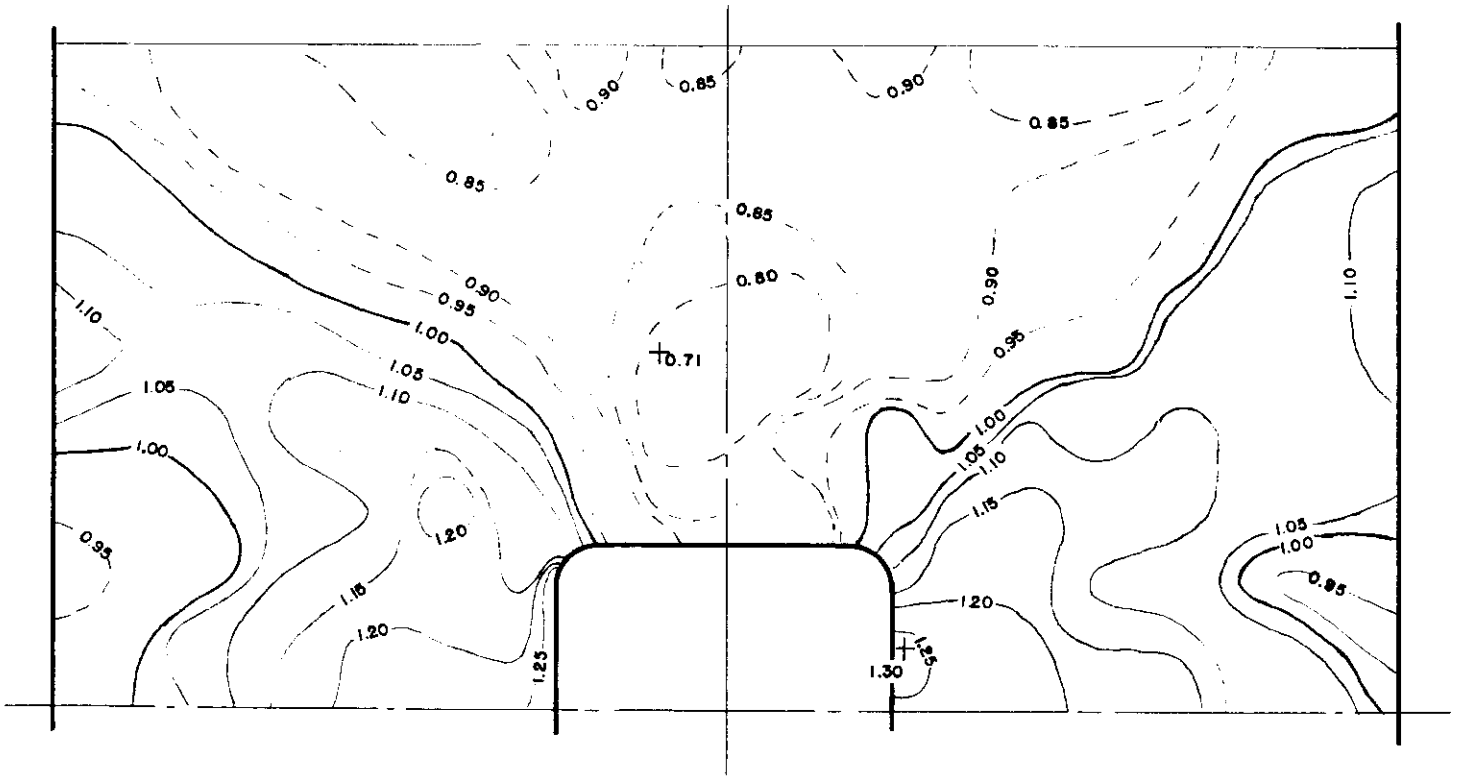


Fig. 25. Contours of the Equal Rates of Energy Absorption. Spec. No. 37.

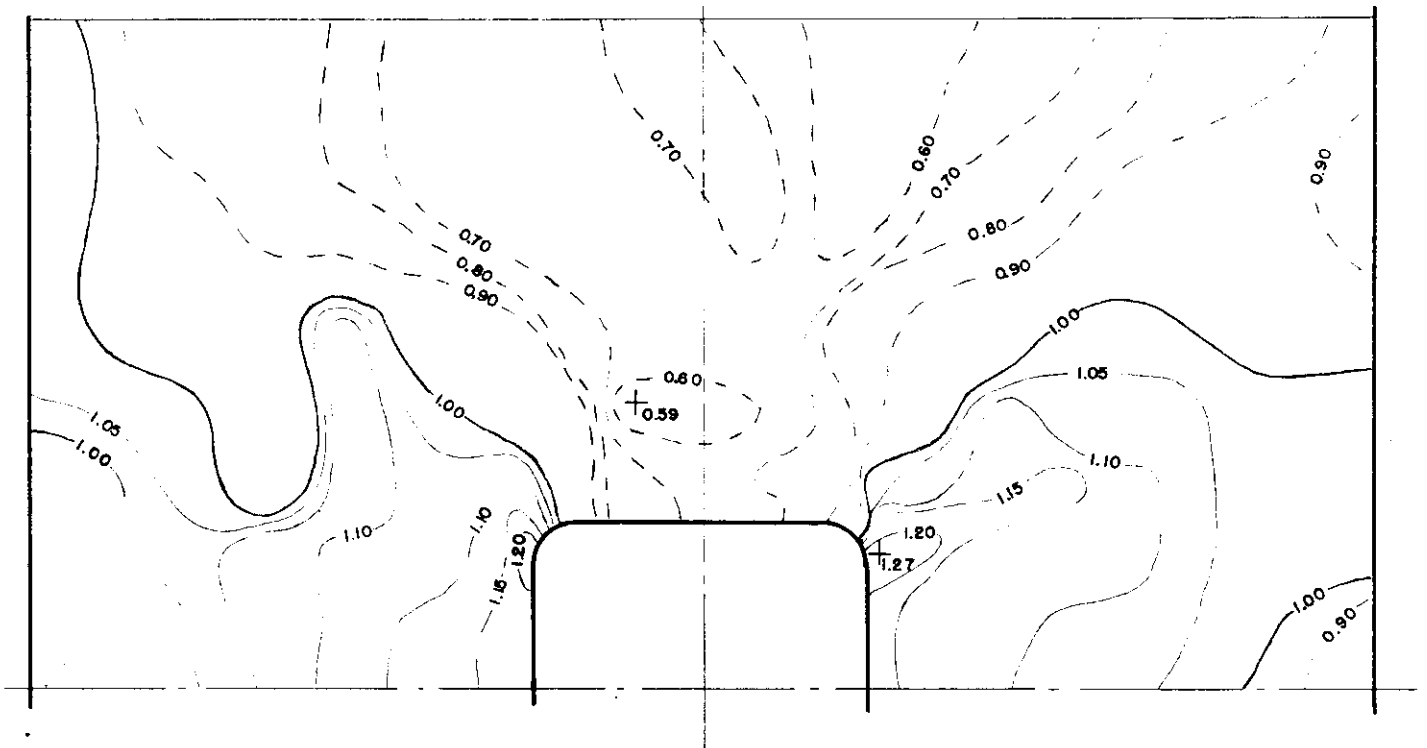


Fig. 26. Contours of the Equal Rates of Energy Absorption. Spec. No. 38.



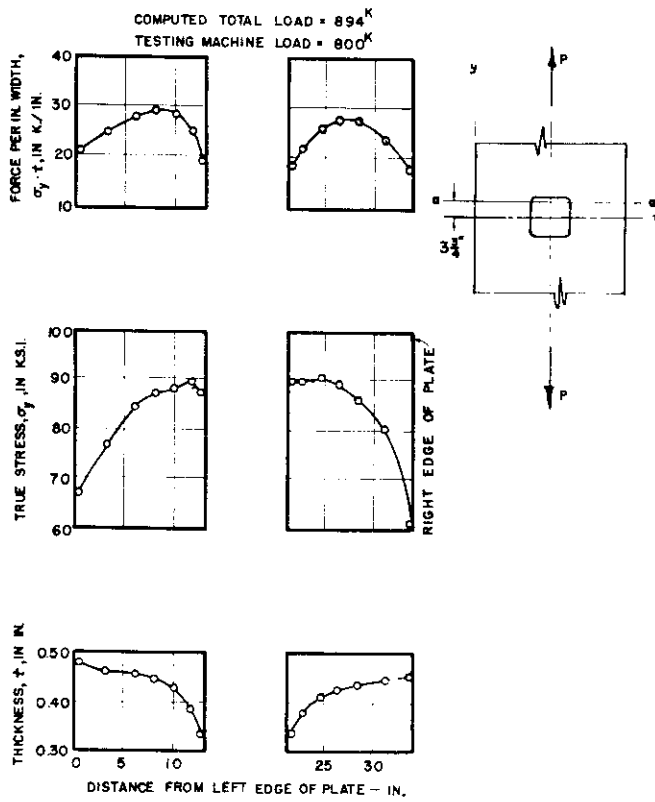


Fig. 27. Distribution of True Thickness, Axial True Stress and Force Per Inch for Transverse Section a-a at Maximum Load of 800 kips. Spec. No. 37.

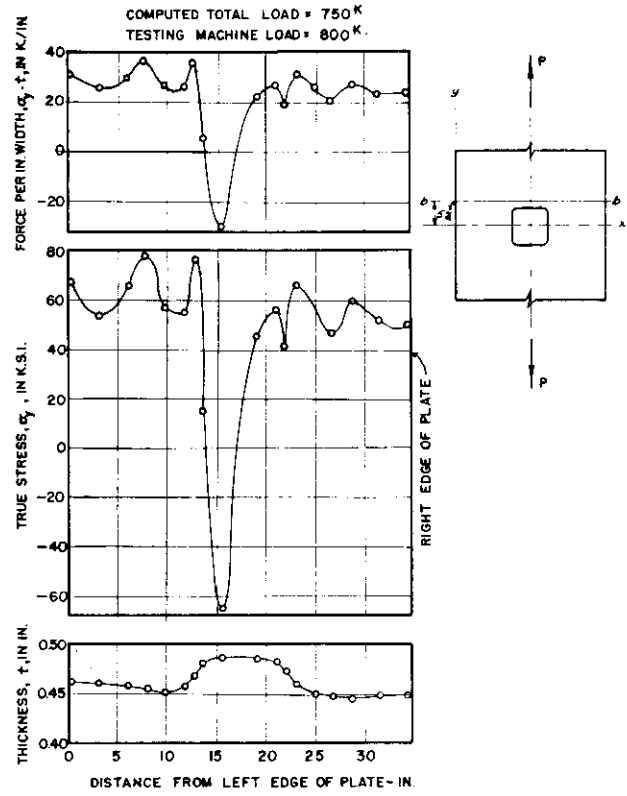


Fig. 28. Distribution of True Thickness, Axial True Stress, and Force per Inch Width for Transverse Section b-b at Maximum Load of 800 kips. Spec. No. 37.

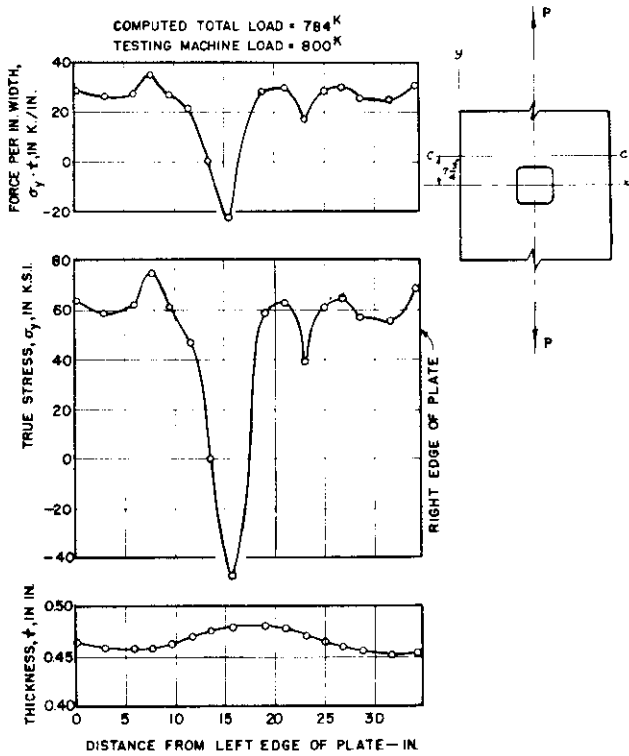


Fig. 29. Distribution of True Thickness, Axial True Stress, and Force per Inch Width for Transverse Section c-c at Maximum Load of 800 kips. Spec. No. 37.

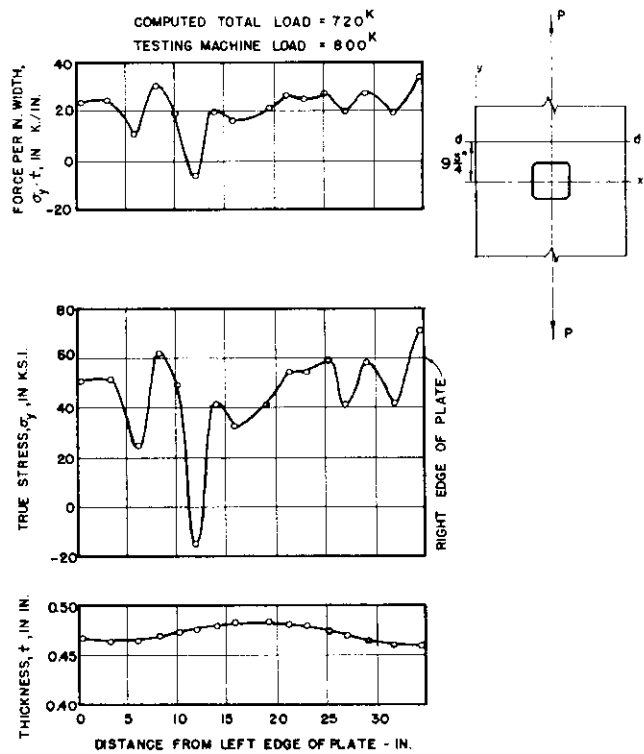


Fig. 30. Distribution of True Thickness, Axial True Stress and Force Per Inch for Transverse Section d-d at Maximum Load of 800 kips. Spec. No. 37.

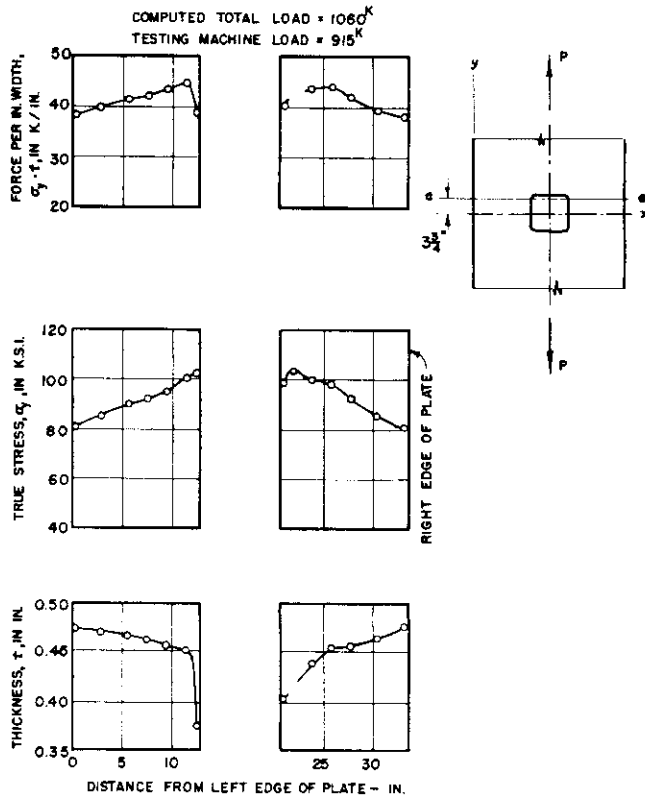


Fig. 31. Distribution of True Thickness, Axial True Stress and Force Per Inch for Transverse Section a-a at Maximum Load of 915 kips. Spec. No. 38.

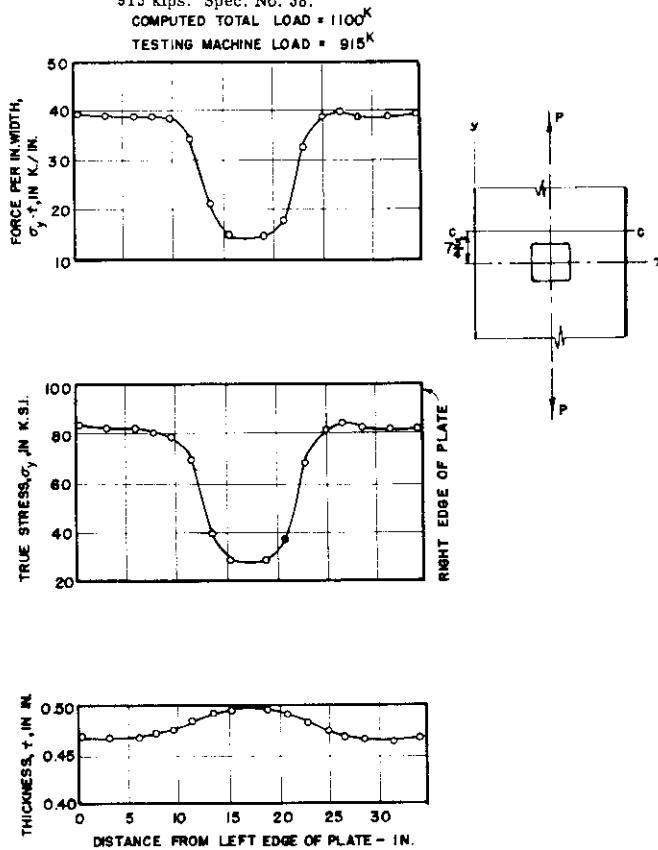


Fig. 33. Distribution of True Thickness, Axial True Stress and Force Per Inch for Transverse Section c-c at Maximum Load of 915 kips. Spec. No. 38.

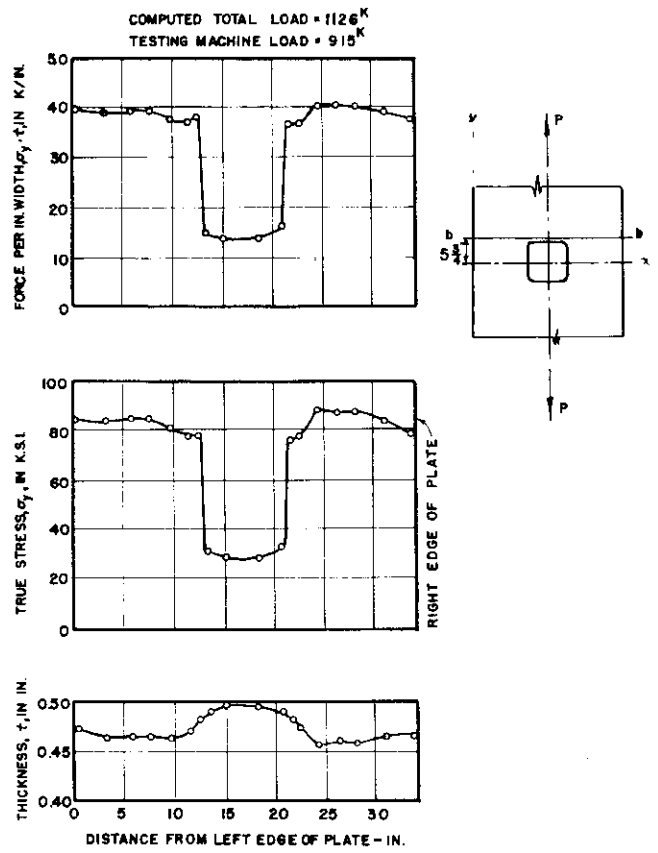


Fig. 32. Distribution of True Thickness, Axial True Stress and Force Per Inch for Transverse Section b-b at Maximum Load of 915 kips. Spec. No. 38.

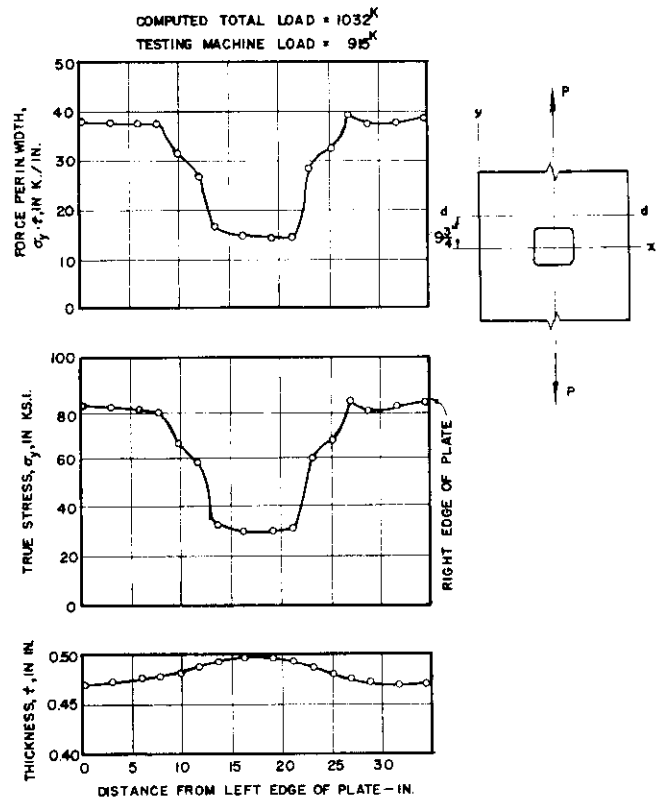


Fig. 34. Distribution of True Thickness, Axial True Stress and Force Per Inch for Transverse Section d-d at Maximum Load of 915 kips. Spec. No. 38.